JOURNAL OF GEOPHYSICAL RESEARCH, VOL. 98, NO. B1, PAGES 447–461, JANUARY 10, 1993

Plio–Pleistocene Time Evolution of the 100-kyr Cycle in Marine Paleoclimate Records

JEFFREY PARK AND KIRK A. MAASCH[1]

Department of Geology and Geophysics, Yale University, New Haven, Connecticut

To constrain theories for the dynamic evolution of global ice mass through the late Neogene, it is important to determine whether major changes in the record were gradual or rapid. Of particular interest is the evolution of the near 100-kyr ice age cycle in the middle Pleistocene. We describe and apply a new technique based on multiple taper spectral analysis which allows us to model the time evolution of quasi-periodic signals. This technique uses both phase and amplitude information and enables us to address the question of abrupt versus gradual onset of the 100-kyr periodicity in the middle Pleistocene. We analyzed three long (> 2.6 m.y.) time series from Deep Sea Drilling Project (DSDP) site 607 (midlatitude Atlantic) and Ocean Drilling Program (ODP) site 677 (equatorial Pacific). The published time scales for these sites differ significantly, influencing the interpretation of the mid-Pleistocene climate transition. When the data series are expressed on the same time scale, there is evidence for a coherent δ^{18}O signal at both sites in the eccentricity and obliquity frequency bands, consistent with variations in global ice volume as the causative factor. If the Shackleton et al. (1990) time scale for ODP 677 is accepted, the amplitude match between the δ^{18}O obliquity cycle and the 65°N insolation derived from the recent astronomical solution of Laskar (1988, 1990) is excellent for times $t \lesssim 2.3$ Ma. If the Ruddiman/Raymo time scale for DSDP 607 is accepted, the 41-kyr δ^{18}O cycle has enhanced amplitude between 1.0 and 1.5 Ma, relative to the late Pleistocene ($t < 1.0$ Ma), implying a nonlinear Earth system response to obliquity insolation cycles. We do not find compelling evidence for an abrupt change in the 100-kyr δ^{18}O signal, although we cannot rule it out at this time. If the Shackleton et al. (1990) time scale for ODP 677 is accepted, our three δ^{18}O records are consistent with a low-amplitude 100-kyr cycle between 1.2 and 2.6 Ma, whose local period of oscillation alternates between the 95- and 124-kyr eccentricity periods, and a gradual increase in the 100-kyr δ^{18}O signal between 0.5 amd 1.0 Ma. The DSDP 607 time scale is more favorable to an abrupt jump in amplitude for the 95-kyr δ^{18}O envelope, but not in the 124-kyr envelope. Rather, long-period δ^{18}O fluctuations appear phase-locked with the 124-kyr eccentricity cycle some 300-400 kyr prior to its growth in amplitude and phase-lock with the 95-kyr eccentricity cycle in the late Pleistocene.

INTRODUCTION

Paleoclimate time series are often dominated by quasi-periodic signals, that is, signals having a dominant oscillation with carrier frequency f_o that suffers amplitude and phase variations on a time scale T_1 much longer (for the most part) than the oscillation period $T_o = 1/f_o$. Such variations have been reported in the spectral properties of Pleistocene time series of paleoclimate proxy variables derived from the marine sedimentary record. The dominant observed carrier frequencies are often those associated with variations in Earth's orbital geometry. These orbital variations are well known as the quasi-periodic Milankovitch cycles: the precession of the equinoxes (major cycles in the range 19-24 kyr), tilt or obliquity (major cycle at 41 kyr) and the eccentricity of Earth's orbit (major peaks in the range 94-126 kyr, at 413 kyr and periods $\gtrsim$2 m.y.). *Shackleton and Opdyke* [1976] noted that during the late Pliocene/early Pleistocene the δ^{18}O variation in core V28-239 is dominated by $\sim$ 40 kyr oscillations, while the late Pleistocene section is dominated by a 100-kyr periodicity. Spectral analyses of other records of δ^{18}O and other ocean-climate indices show similar behavior [e.g., *Pisias and Moore*, 1981; *Start and Prell*, 1984; *Ruddiman et al.*, 1986a,b]. Spectra of late Pleistocene δ^{18}O typically show a dominant peak at approximately 100 kyr, phase-locked with the eccentricity cycles in this frequency band, along with smaller peaks at frequencies corresponding to changes in both obliquity and precession (with periods near 41 kyr and 23 and 19 kyr, respectively). On the other hand, spectra of early Pleistocene records appear to be dominated by $\sim$ 41 kyr periodicity [e.g., *Raymo et al.*, 1989; *DeBlonde and Peltier*, 1991]. Higher-resolution cores currently becoming available suggest that there may have also been considerable variation in the precessional band during the early part of the Pleistocene.

The response of Earth's climate to long-term changes in its boundary conditions can be illuminated by studying its response to the changes in received solar energy associated with orbital variations. Precession is associated with insolation anomalies up to 10% from the mean at the orbital apogee and perigee (the yearly mean anomaly largely cancels). Changes in obliquity vary the location of the Arctic and Antarctic circles over a total range of $\sim$ 2.5°, affecting principally the wintertime insolation at high latitudes. Change in orbital eccentricity affects insolation principally by modulating the strength of the precession cycle and has a relatively small direct influence on the solar energy reaching Earth. If the response of Earth's climate system to insolation variations were linear with a slowly varying frequency domain transfer function, obliquity and precession periods would dominate the records of climate proxy variables. A time-dependent linear Earth system response, governed by slow changes in, e.g., continental placement and elevation, would likely lead to slow variations in the spectral amplitudes of climate proxy variables at Milankovitch frequencies.

[1]Now at Institute for Quaternary Studies, University of Maine Orono.

Paper number 92JB01815.
0148-0227/93/92JB-01915$05.00

The dominant ~ 100-kyr ice age cycle in the late Pleistocene remains an outstanding problem for which there is no universally accepted solution. To develop a theory that explains the time evolution of the 100-kyr ice age cycle, it is relevant to study the timing and nature of the cycle's onset, which is thought to have occurred sometime in the interval 0.5-1.0 Ma. For instance, was the onset of the 100-kyr cycle gradual or sudden? A sudden onset would characterize a bifurcation in a nonlinear system [*Maasch and Saltzman*, 1990; *Saltzman and Maasch*, 1990, 1991; *Matteucci*, 1991] and would support the existence of a fundamental instability in the climate system. A gradual increase in ice age cycle intensity could, by contrast, suggest a shift in an otherwise stable climate regime or the steady growth of an unstable oscillation [e.g., *Saltzman and Sutera*, 1987], perhaps triggered by a late Cenozoic downdraw of atmospheric CO_2, or perhaps the interaction of ice sheet growth with the viscous response of the mantle to applied loads [e.g., *Le Treut and Ghil*, 1983; *DeBlonde and Peltier*, 1990, 1991].

In this paper we present a new time series analysis technique, which we call envelope inversion, as a method for addressing the long-term variability in Earth climate's interaction with its orbital cycles. *Maasch* [1988] and *DeBlonde and Peltier* [1991] have applied statistical tests to δ^{18}O data series to evaluate the hypothesis that the mean and variance suffered an abrupt change in the mid-Pleistocene. Both studies found evidence for an abrupt change in the mean of a collection of δ^{18}O records at 0.85-0.90 Ma, consistent with a sudden cooling of mean global temperature. *Maasch* [1988] also found evidence supporting an abrupt increase in δ^{18}O variance in several records, coincident in time with the inferred jump in the mean, consistent with a sudden increase in climate variability. *DeBlonde and Peltier* [1991] did not find a coincident abrupt jump in δ^{18}O variance at the mid-Pleistocene transition using data from Deep Sea Drilling Project (DSDP) site 607 and Ocean Drilling Project (ODP) site 677, using identical statistical tests. (*Maasch* [1988] also examined the benthic δ^{18}O series from DSDP site 607 and found no evidence for an abrupt change in variance.) "Variance fluctuation" was interpreted by these studies as a proxy for the amplitude of the 100-kyr δ^{18}O cycle, the putative ice sheet cycle. The techniques developed in this paper facilitate the study of time-dependent data variance in narrow frequency bands, so that the 100-kyr δ^{18}O cycle can be examined more directly. In addition to examining the time-evolution of the 100-kyr δ^{18}O cycle, we can address related questions, such as (1) how is the 100-kyr cycle related to climate variation at other orbital periods? (2) To what extent does the climate proxy record suggest a linear response of the Earth system at the other orbital periods?

The mathematical formulation of "envelope inversion" leads to a linear inverse problem with a finite number of data [e.g., *Parker*, 1977; *Menke*, 1984], where the "data" are spectrum estimates drawn from a narrow bandwidth around the carrier frequency f_o. Solutions to linear inverse problems are nonunique, leading to limitations and opportunities often not explored in time series algorithms. Formally, an infinite number of "envelopes" will fit the data. In practice, only a restricted subset of solutions will be slowly varying, and one can modify the calculation to find the "smoothest" envelope consistent with the data. This estimator is more flexible than the more standard complex-demodulate envelope estimator, which is shown to be the "smallest" envelope (in an root-mean-square sense) consistent with the spectral data. In the next section we outline the linear inverse problem for estimating the envelope of quasi-periodic signals in paleoclimate time series, using test series to illustrate the behavior of the algorithm. Then we analyze three data series from two long, high-resolution marine sediment cores to examine the evolution of climate-proxy behavior at Milankovitch frequencies corresponding to eccentricity, obliquity and precession, with particular attention to the 100-kyr ice age cycle.

ENVELOPE ESTIMATION

We outline the inversion algorithm briefly. A condensed derivation is given by *Park* [1990], and a more detailed discussion is given by *Park* [1992]. An isolated discretely sampled quasi-periodic signal can be expressed in the form $x_n = \Re\{A_n e^{-2\pi i f_o n\Delta t}\}$, $n = 1, 2, \ldots N$ for a time series of duration $T = N\Delta t$. The slowly varying complex-valued envelope $A_n = A(n\Delta t)$ can be represented as a narrow-band function $\bar{A}(f)$ in the frequency domain, in particular,

$$A(n\Delta t) = A_n = \Delta t \int_{-f_N}^{f_N} \bar{A}(f) e^{-2\pi i f n\Delta t}\, df, \qquad (1)$$

where $f_N = 1/(2\Delta t)$ is the Nyquist frequency. The Δt prefactor specifies identical "units" for $A(t)$ and $\bar{A}(f)$ and corrects a typographical error in *Park* [1992]. We assume that $\bar{A}(f) \approx 0$ for $|f| > f_w$ for some half-bandwidth f_w, so that it has minimum time scale of variation $T_1 = 1/f_w$. If the envelope of a quasi-periodic signal undergoes one or more rapid changes, such behavior "broadens" $\bar{A}(f)$ outside the interval $|f| \le f_w$. In principle, this low-amplitude spectral information can be used to help reconstruct the signal. In practice, in paleoclimate series the quasi-periodic signal is one component of a "mixed" spectrum containing a significant stochastic broadband component. Often $|\bar{A}(f)|$ is comparable to the broadband "background" spectrum outside some narrow bandwidth $[-f_w, f_w]$, so that one is faced with reconstructing the envelope A_n, $n = 1, 2, \ldots N$, from spectral information inside $[-f_w, f_w]$ only.

As a basis set for expanding $\bar{A}(f)$ over $[-f_w, f_w]$, we use the discrete prolate spheroidal wavefunctions $W_k(f)$ [*Thomson*, 1982; *Slepian*, 1983]. The $W_k(f)$ are the discrete Fourier transform pairs of Slepian tapers $w_n^{(k)}$, $n = 1, \ldots N$

$$\begin{aligned} W_k(f) &= \textstyle\sum_{n=1}^{N} w_n^{(k)} e^{2\pi i f n\Delta t} \\ w_n^{(k)} &= \Delta t \int_{-f_N}^{f_N} W_k(f) e^{-2\pi i f n\Delta t}\, df \\ &= \frac{\Delta t}{\lambda_k} \int_{-f_w}^{f_w} W_k(f) e^{-2\pi i f n\Delta t}\, df \end{aligned} \qquad (2)$$

and satisfy the condition that the functional

$$\lambda(W) = \frac{\displaystyle\int_{-f_w}^{f_w} |W(f)|^2\, df}{\displaystyle\int_{-f_N}^{f_N} |W(f)|^2\, df} \qquad (3)$$

is stationary. Larger stationary values of the functional $\lambda_k = \lambda(W_k)$ occur for functions $W_k(f)$ that are concentrated in

the narrow band $[-f_w, f_w]$. Tapers with $\lambda \approx 1$ can be used to construct spectrum estimates that are resistant to spectral leakage. If $f_w = pf_R$, where $f_R = 1/T = 1/(N\Delta t)$ is the Rayleigh frequency of the time series, the first $2p-1$ eigentapers have sufficient spectral leakage resistance to be useful in spectrum analysis. Tapers constructed for $f_w = pf_R$ (p need not be an integer) are called $p\pi$-prolate Slepian tapers, following the terminology of *Thomson* [1990]. Envelope inversion can be expressed using other direct spectrum analysis techniques (e.g., using adjacent frequency estimates of a boxcar-tapered fast Fourier transform (FFT)), but the Slepian tapers offer better statistical properties [e.g., *Park et al.*, 1987].

If $A(f) = 0$ outside the narrow band $[-f_w, f_w]$, the behavior of $\bar{A}(f)$ that is resolvable with the N-point data series is an expansion of N prolate spheroidal wavefunctions:

$$\bar{A}(f) = \sum_{k=0}^{N-1} a_k W_k(f) \tag{4}$$

for $|f| \le f_w$, so that $A(n\Delta t) = A_n$ and

$$A_n = \Delta t \sum_{k=0}^{N-1} \int_{-f_w}^{f_w} a_k W_k(f) e^{-2\pi i f n \Delta t}\, df = \sum_{k=0}^{N-1} \lambda_k a_k w_n^{(k)}. \tag{5}$$

The coefficient a_k is related directly to the DFT of the data series $x_1, x_2, \ldots, x_N$ tapered by the kth Slepian taper $w_n^{(k)}$, also known as the kth eigenspectrum estimate $Y_k(f)$, evaluated at f_o:

$$Y_k(f_o) = \sum_{n=1}^{N} w_n^{(k)} x_n e^{2\pi i f_o n \Delta t} = \sum_{n=1}^{N} w_n^{(k)} A_n = \lambda_k a_k. \tag{6}$$

Note that $Y_k(f_o)$ is a complex valued quantity: its squared-modulus is a positive-definite squared-spectrum estimator. In practical situations one must truncate (6) at some $K \lesssim 2p-1$ to minimize spectral leakage bias. For some chosen truncation K, we can estimate the envelope A_n with $B_n, n = 1, \ldots N$, where

$$B_n = \sum_{k=0}^{K-1} \lambda_k^{-1} Y_k(f_o) w_n^{(k)}. \tag{7}$$

This is the multitaper complex demodulate at the carrier frequency f_o [*Thomson*, 1990].

Equation (7) is a valid model for the oscillation envelope A_n, but it is not the only valid model. For instance, a constant envelope $A_n \equiv A_o$ cannot be represented by any weighted sum of the first few Slepian tapers, but often is a most excellent physical model. More flexibility is gained by treating the estimation of A_n as a standard linear inverse problem [*Parker*, 1977; *Menke*, 1984]. Designate $\mathbf{B} = (B_1, B_2, \ldots, B_N)$ as the estimate, or "model," for the "true" oscillation envelope $\mathbf{A} = (A_1, A_2, \ldots, A_N)$. We obtain $\mathbf{B}$ as the solution to a linear inverse problem. The leakage-resistant eigenspectrum estimates are recast as K "data constraints:"

$$Y_k(f_o) = \sum_{n=1}^{N} w_n^{(k)} A_n = \mathbf{g}_k \cdot \mathbf{A}, \tag{8}$$

which identify K data kernels $\mathbf{g}_k = \mathbf{w}_k$. It is a standard consequence of the projection theorem in inner-product spaces that the model $\mathbf{B}$ that fits the K data constraints exactly, while minimizing $\|\mathbf{B}\|^2 = \mathbf{B} \cdot \mathbf{B}$, is a linear combination of the data kernels $\mathbf{g}_k$ and is the complex demodulate given by (7). Therefore, the complex demodulate is the minimum-size solution to the data constraints. Define a data vector $\mathbf{y} = (Y_0(f_o), \ldots, Y_{K-1}(f_o))$, a coefficient vector $\mathbf{a} = (a_0, \ldots, a_{K-1})$, and a $K \times N$ kernel matrix $\mathbf{G}$ whose rows are the data kernels $\mathbf{g}_k$. If we form a Gram matrix $\mathbf{\Gamma} = \mathbf{G} \cdot \mathbf{G}^{\mathbf{T}}$, where $\Gamma_{kl} = \mathbf{g}_k \cdot \mathbf{g}_l$, the formal solution for this expansion is $\mathbf{a} = \mathbf{\Gamma}^{-1} \cdot \mathbf{y}$. In the minimum-size solution (7), the orthogonality of the Slepian tapers renders the Gram matrix $\mathbf{\Gamma}$ diagonal.

Once the linear inverse problem is formulated, other solutions $\mathbf{B}$ can be found that minimize other quadratic functionals. For instance, one can solve for an envelope that deviates least from some preferred model $\mathbf{w}^{(0)}$, e.g., a constant envelope. To obtain smooth envelopes consistent with measured eigenspectra, we use a variation of Occam's inversion [*Constable et al.*, 1987] suggested by R. L. Parker (unpublished manuscript, 1992). Consider the approximate first-difference operator $\mathbf{D} = D_{ij}$, an $N \times N$ matrix with $D_{11} = \epsilon \ll 1$, $D_{ii} = 1$ for $i > 1$; $D_{i-1,i} = -1$ and $D_{ij} = 0$ otherwise. The inverse of this matrix is a crude integration operator $\mathbf{D}^{-1}$, where $D_{1i}^{-1} = \epsilon^{-1}$, $D_{ij}^{-1} = 1$ for $1 < i \le j$ and $D_{ij}^{-1} = 0$ for $j < i$. The data constraints (8) can be rewritten as

$$Y_k(f_o) = \mathbf{w}_k \cdot \mathbf{D}^{-2} \cdot \mathbf{D}^2 \cdot \mathbf{A} = \tilde{\mathbf{g}}_k \cdot \tilde{\mathbf{A}} \tag{9}$$

where $\tilde{\mathbf{g}}_k = \mathbf{w}_k \cdot \mathbf{D}^{-2}$ and $\tilde{\mathbf{A}} = \mathbf{D}^2 \cdot \mathbf{A}$. An envelope $\mathbf{B}$ that satisfies the data constraints while minimizing

$$\begin{aligned} \|\mathbf{D^2} \cdot \mathbf{B}\|^2 \;=\; & \textstyle\sum_{n=2}^{N-1} \big\{ (B_{n+1} - 2B_n + B_{n-1})^2 \\ & + (B_2 - (1+\epsilon)B_1)^2 + \epsilon^4 B_1^2 \big\} \end{aligned} \tag{10}$$

can be constructed from $\mathbf{D}^{-2} \cdot \tilde{\mathbf{B}}$, where $\tilde{\mathbf{B}}$ is a linear combination of the $\tilde{\mathbf{g}}_k$. The first term on the right-hand side of (10) measures the roughness of the envelope. The extra terms in (10) complicate interpreting $\mathbf{B} = \mathbf{D}^{-2} \cdot \sum_{k=0}^{K-1} \tilde{a}_k \tilde{\mathbf{g}}_k$ as the smoothest model for the oscillation envelope $\mathbf{A}$. In numerical examples their influence on the solution roughness appears negligible for $N > 100$ data points and $\epsilon \lesssim 10^{-4}$. The extra terms penalize envelope models for which $\sum_{n=2}^{N-1} (B_{n+1} - 2B_n + B_{n-1})^2 = 0$ e.g., constant vectors and linear ramps. P. Stark (personal communication, 1992) has suggested that an alternative roughness penalty function can be constructed by expressing the envelope estimate in terms of spline functions [e.g., *Constable and Parker*, 1988]. With a spline representation, one can effect an explicit constraint on the second derivative of the continuous-time envelope, unlike the discretized constraint offered by (10). In practice, the distinction between the use of (10) and of a spline-based penalty function should be negligible for nearly all time series applications, because the discrete envelope estimate $\mathbf{B}$ is sampled densely, relative to the number of spectral data constraints.

Four extensions of the above development are useful:

1. The first-difference matrix $\mathbf{D}$ can be partitioned at a chosen breakpoint $\tilde{N} < N$, which allows envelopes to have discontinuities at the chosen breakpoint but constrains them to be smooth elsewhere.

2. Climate proxy records often have segments of missing data due to coring gaps or hiatuses in sedimentation. The

effect of gaps on spectrum estimates can be modelled by introducing identical gaps in the tapers $\mathbf{w}_k$. An envelope estimate derived from the smoothness penalty functional (10) will interpolate the gap with a sum of a third-order polynomial and the fixed element $\mathbf{w}^{(0)}$.

3. The desired carrier frequency f_o need not equal one of the discrete frequencies of the numerical Fourier transform. If we choose eigenspectra $Y(\hat{f}_o)$ at a nearby FFT frequency $\hat{f}_o$ for analysis, the K data kernels $\mathbf{g}_k$ in (8) become complex-valued vectors and the Gram matrix $\mathbf{\Gamma}$ becomes complex-Hermitian rather than real-symmetric. Otherwise the solution algorithm is similar.

4. Stochastic processes may contribute significantly to the eigenspectrum estimates $Y_k(f_o)$, and can be interpreted as "uncertainties" in the spectral data. A standard tactic is to allow a specified misfit to the data $S^2 = \sum_k (Y_k(f_o) - \tilde{Y}_k)^2$, where $\tilde{Y}_k$ is the kth model prediction, while minimizing the penalty functional $\|\mathbf{B}\|^2$ or (10). Details of this method are given by *Shure et al.* [1982], in which the constrained optimization is set up with a Lagrange multiplier μ. The effect of a locally white background is roughly equivalent for leakage-resistant eigenspectrum estimates, so that the misfit to each $Y_k(f_o)$ can be assumed to have equal variance. However, if the roughness penalty (10) is used, the contribution of the more oscillatory higher-order Slepian tapers to the solution will be diminished relative to that of the low-order tapers. Details are described by *Park* [1992]. We do not allow data misfit in the analysis described below, but this generalization of the envelope inverse algorithm will be important for weaker signals and for simultaneous "cross-spectral" envelope estimates using multiple records.

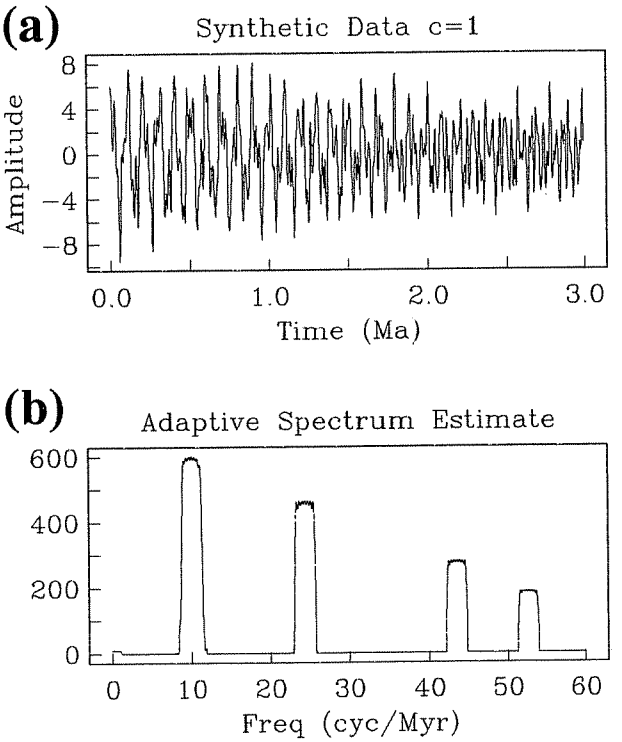

Fig. 1. Synthetic test with gradual amplification of the 100-kyr oscillation. (*a*) The data series, 1000 samples with sampling interval 3 kyr. (*b*) The adaptive multiple-taper spectrum estimate, using seven 4π-prolate Slepian eigentapers.

SYNTHETIC TIME SERIES

We apply envelope estimation to several synthetic time series with characteristics similar to the paleoclimate record. Consider synthetic time series of the form

$$x(t) = \sum_{i=1}^{4} A_i(t) \sin[2\pi f_i + \phi_i(t)]. \qquad (11)$$

The amplitudes, A_i, $i = 1, \ldots, 4$, and frequencies, f_i, $i = 1, \ldots, 4$, are chosen to generate a time series with properties similar to observed $\delta^{18}O$ records. In particular, we fix $f_1 = 1000/100 = 10$ cycles/m.y., $f_2 = 1000/41 = 24.4$ cycles/m.y., $f_3 = 1000/23 = 43.5$ cycles/m.y., $f_4 = 1000/19 = 52.6$ cycles/m.y., $A_2(t) = 2.5$, $A_3(t) = 1.5$, $A_4(t) = 1.0$, and $\phi_2(t) = \phi_3(t) = \phi_4(t) = 0.0$. Time variations in $A_1(t)$ and $\phi_1(t)$ are imposed to generate an abrupt or gradual change in the complex amplitude of the 10 cycles/m.y. cycle. We constructed 3 m.y. synthetic records using (11) with

$$\begin{aligned} A_1(t) &= 3 - 2\tanh[c(t-1.5)] \\ \phi_1(t) &= -\pi \tanh[c(t-1.5)]/4 \end{aligned} \qquad (12)$$

where t is time in million years before the present (Ma) and c controls the rate of change in the 100-kyr amplitude and phase near the transition point at 1.5 Ma. The sample time is 3 kyr, so that the series each have $N = 1000$. When $c \ll 1$, both amplitude and phase in the 100-kyr band are roughly constant over the record at values of $A_1(t) = 3.0$ and $\phi_1(t) = 0.0$. For $c = 1$, the amplitude $A_1(t)$ varies smoothly from a low value near 1.2 at 3 Ma to 4.8 at 0 Ma, while $\phi_1(t)$ varies smoothly from $-40°$ to $40°$. In contrast, for $c = 10000$ both the amplitude and phase suffer an abrupt change at 1.5 Ma, but are essentially constant elsewhere.

The synthetic time series constructed using (11) and (12) for $c = 1$ is shown in Figure 1*a*, along with the multitaper spectrum estimate with seven 4π-prolate Slepian tapers $\mathbf{w}_k$ (Figure 1*b*). For this synthetic time series we have constructed three models for the envelope of the 100-kyr oscillation, each using seven 4π-prolate Slepian tapers $\mathbf{w}_k$ and a constant fixed element $\mathbf{w}^{(0)}$: a smallest envelope (akin to the complex demodulate); a smoothest envelope using the penalty function (10), and a smoothest envelope with a breakpoint allowed at $t = 1.5$ Ma. Figure 2 graphs the estimated amplitude and phase of $A(t)$ against the theoretical values. The smooth model for the envelope successfully estimates the true amplitude and phase of the 100-kyr cycle in the synthetic time series (Figure 1*a*), while the "smallest" envelope has spurious fluctuations. The envelope solution with a discontinuous break is similar to the continuously smooth envelope solution. Although not shown, the changes in amplitude and phase in the 100-kyr band have negligible effect on envelope estimates for the other orbital cycles.

Figure 3 shows the time series and the multitaper spectrum estimate for the case where $A_1(t)$ and $\phi_1(t)$ both increase abruptly at $t = 1.5$ Ma ($c = 10000$). Note that the envelope discontinuity is manifest as a "talus slope" at the base of the boxy spectral peak at 10 cycles/m.y. This low-amplitude feature would likely be obscured in the spectrum estimate of a realistically noisy data series. The smallest and smoothest envelopes consistent with eigenspectra at $f = 10$ cycles/m.y. are shown in Figure 4 along with the theoretical values for $A_1(t)$ and $\phi_1(t)$. Both continuous-envelope

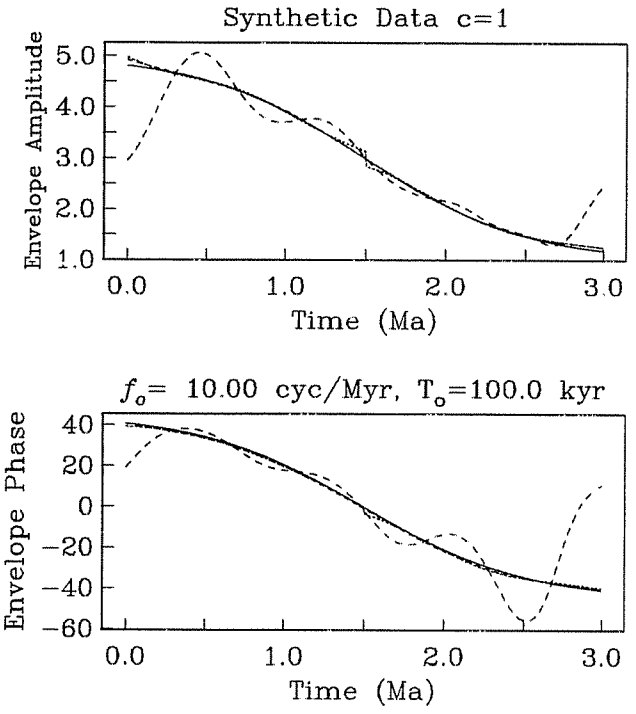

Fig. 2. Envelope inversions for the time evolution of the 100-kyr signal in the synthetic data graphed in Figure 1. The solid curve graphs the theoretical amplitude and phase. The long-dashed curve graphs the "minimum size" envelope that fits exactly the seven eigenspectra $Y_k(f_o)$, evaluated at carrier frequency $f_o = 10$ cycles/m.y. The short-dashed curve graphs the smoothest envelope, in the sense of minimizing the numerical second derivative, that fits the spectral data exactly. The medium-dashed curve is the smoothest envelope with a discontinuity allowed at $t = 1.5$ Ma. Note that this solution differs little from the smoothest envelope, confirming that the data series does not prefer an abrupt change in the envelope.

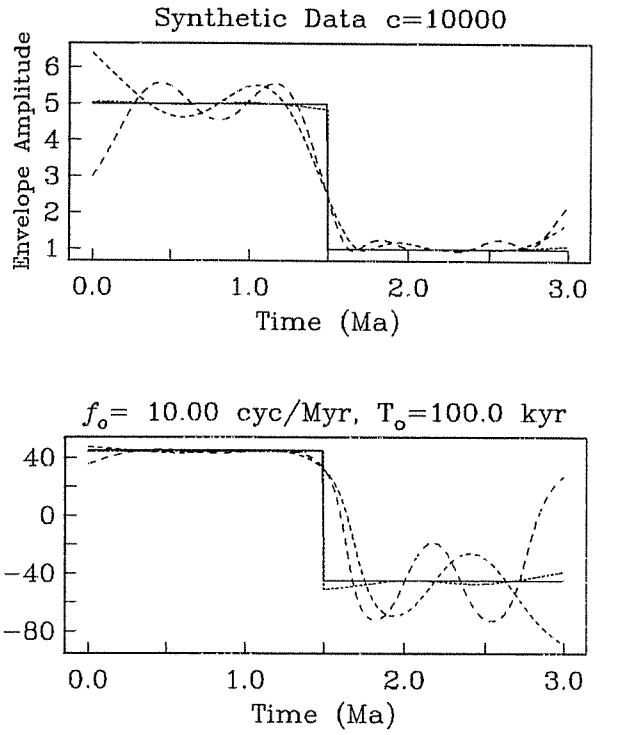

Fig. 4. Envelope inversions for the time evolution of the 100-kyr signal in the synthetic data graphed in Figure 3. The solid curve graphs the theoretical amplitude and phase. The long- and short-dashed curves graph the "minimum size" and smoothest envelopes, respectively, that fit exactly the seven eigenspectra $Y_k(f_o)$, evaluated at carrier frequency $f_o = 10$ cycles/m.y. The medium-dashed curve is the smoothest envelope with a discontinuity allowed at $t = 1.5$ Ma. Note that this solution differs greatly from the continuous envelopes, confirming that the data series prefers an abrupt change in the envelope.

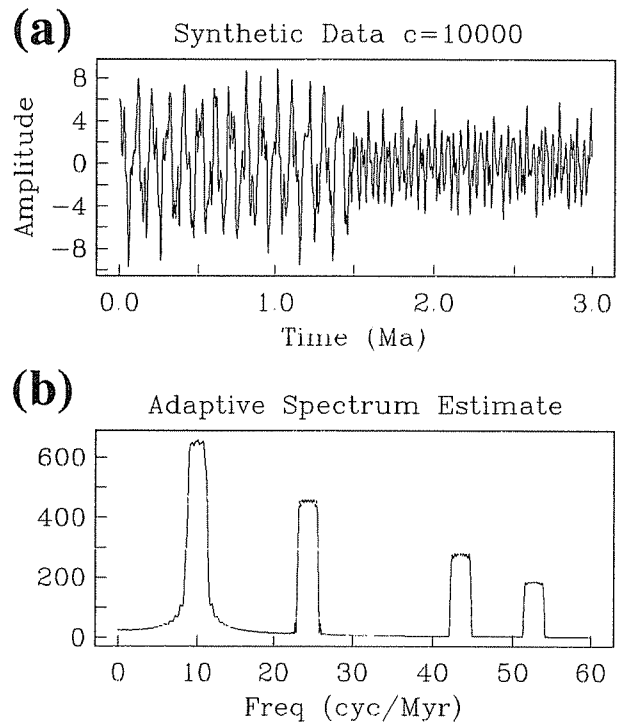

Fig. 3. Synthetic test with sudden amplification of the 100-kyr oscillation. (*a*) The data series. (*b*) The adaptive multiple-taper spectrum estimate, using seven 4π-prolate Slepian eigentapers.

models detect a rapid change in phase near the midpoint of the series, but only the inversion that allows a breakpoint follows well the abrupt change in $A_1(t)$ (Figure 4, dashed). An incorrect choice of breakpoint leads to much more complicated models: tests suggest that the location of a break can be determined to a precision of $< 5\%$ of the total series duration if the signal to noise is large.

All of the above solutions fit the data (the eigenspectra $Y(f_o)$) within numerical precision. Infinitely many envelopes will fit the data equally well, because the inverse problem for $A(t)$ is nonunique. A large proportion of this infinity of models, however, correspond to $\bar{A}(f)$ with large amplitude outside $[-f_w, f_w]$. In practical situations it is prudent for interpretation to use the smoothest model that fits the data, for it suppresses features that are not required by the data and leads to models that are reasonably bandlimited. The second-derivative penalty, however, sometimes leads to solutions with spurious linear ramps at one or both ends of the series. In such cases, an inversion with a first-derivative constraint (equations (9) and (10) with the matrix $\mathbf{D}$ to the first power) can be calculated as a crosscheck. Unusual behavior, such as abrupt changes in amplitude and phase, can suggest rapid change or discontinuities in the envelope. Variations of the above strategies may be useful in some applications, especially when comparing the behavior of multiple data series. For instance, one could solve for a single envelope that fits narrow-band spectral data from multiple data series, if one allows for some misfit due to in-

coherent noise processes. We defer the development of such applications to a later contribution.

ENVELOPE ANALYSIS OF MARINE $\delta^{18}O$ RECORDS

We analyzed data series of $\delta^{18}O$ (Table 1) from two long, high-resolution drill cores: ODP 677 from the eastern equatorial Pacific at 1°12'N, 83°44'W and DSDP 607 from the mid-latitude North Atlantic at 41°00'N, 32°58'W. Comparing two sites introduces the problem of placing the data series on an identical time scale. Isotope measurements are made from core samples with irregular spacing in depth, and the sediment accumulation rate is not constant with either time or geographic location. An absolute time reference can be obtained at magnetic reversals within the core by radiometric dating, and at intermediate times by "tuning" to the phase of the Milankovitch cycles. However, both measures of absolute time are themselves undergoing revision, so that the published $\delta^{18}O$ time scales from sites 607 and 677 use different astronomical calculations for the orbital cycles and infer different dates for the Bruhnes-Matayama magnetic reversal (in the range 0.73–0.78 Ma). As we illustrate below, it is possible to place the data series on a common time scale. This effort is rewarded by a surprising agreement between sites on the time-evolution of the 100-kyr $\delta^{18}O$ cycle. Moreover, we argue that the choice of one core's time scale over the other's has significant implications for the longterm dynamics of global climate.

Shackleton and Hall [1989] produced both benthic and planktonic $\delta^{18}O$ records for ODP 677 with a sampling interval of 10 cm (additional measurements were subsequently reported by *Shackleton et al.* [1990]). The average sedimentation rate at ODP site 677 is roughly 4 cm/kyr and the length of the core is 113 m. Thus, the $\delta^{18}O$ records from ODP 677 span roughly 2.6 m.y. and have a time resolution $\Delta t \approx 2.5$ kyr. The $\delta^{18}O$ record from DSDP 607 was measured using benthic foraminifera [*Ruddiman et al.*, 1989; *Raymo et al.*, 1989] at a sampling interval of 15 cm. With an average sedimentation rate of 4.5 cm/kyr and a core length of 122 m, the $\delta^{18}O$ record from DSDP 607 spans approximately 2.8 m.y. with a time resolution of about 3.5 kyr. Figure 5 shows the three data series from sites 607 and 677 against the insolation curve at 65°N latitude given by *Berger and Loutre* [1991]. The published time scales (*Ruddiman et al.* [1989] and *Raymo et al.* [1989] for DSDP 607 and *Shackleton et al.* [1990] for ODP 677) are used for the data series in this comparison. The time scale for DSDP 607 was developed using the same approach as SPECMAP [*Imbrie et al.*, 1984], by tuning an initial time scale (based on paleomagnetic stratigraphy) to a target curve constructed by phase lagging the obliquity and precession curves of *Berger* [1978]. In particular, obliquity is lagged by 8 kyr and precession is lagged by 5 kyr. The time scale for ODP 677 was also tuned, but in this case to the updated 65°N insolation curve of *Berger and Loutre* [1991], based on the astronomical solutions of *Laskar* [1988, 1990]. Rather than simply phase lag the obliquity and precession, the target curve was constructed using the model of *Imbrie and Imbrie* [1980].

We used spline interpolation with allowed misfit [*Reinsch*, 1967] to produce evenly spaced time series, free from spurious "overshoots." To calibrate the two time scales used for the DSDP 607 and ODP 677 data, we correlated the $\delta^{18}O$ isotope "stages" 1–100 by visual identification (Figure 6). Over the last 0.6 m.y. the two time scales are roughly equivalent. However, between 0.6 and 1.2 Ma the age estimates of oxygen isotope stages on these time scales diverge. For ages > 1.2 Ma, $\delta^{18}O$ stage ages on the ODP 677 scale average about 130 kyr older than on the DSDP 607 scale. This major difference proposed by *Shackleton et al.* [1990] depends only weakly on phase shifts in the newer astronomical calculation but instead reflects a different interpretation of the correlation of the orbital cycles (used in tuning) with the $\delta^{18}O$ record between 0.6 and 1.2 Ma. Since these age shifts straddle the mid-Pleistocene climate transition, the choice of time scale influences the transition in the $\delta^{18}O$ record.

Figure 7 compares spectrum estimates of the four series shown in Figure 5 using the multitaper adaptive spectrum estimator [*Thomson*, 1982; *Park et al.*, 1987] with seven 4π-prolate Slepian tapers. The normalization for the insolation series was chosen to obtain rough parity in the amplitude of the obliquity peak at 41-kyr period. The squarish profile of the obliquity peaks diagnoses phase coherent signals. Note the predominance of precession frequencies at $40 < f < 60$ cycles/m.y. in the 65°N insolation record relative to a paucity of energy in the eccentricity band near $f = 10$ cycles/m.y. By contrast, the $\delta^{18}O$ spectra have prominent peaks near $f = 10$ cycles/m.y. which exceed greatly the amplitude in the precession band. The peaks near 10 cycles/m.y., however, are not box-shaped, suggesting that the signal in this band is only weakly phase coherent. This observation is confirmed by applying an F variance ratio line detection test [*Thomson*, 1982, 1990; *Park and Herbert*, 1987; *Berger et al.*, 1991]. Spectral peaks at $f \approx 24.4$ cycles/m.y., presumably related to obliquity variations, have F test values > 25 for the three data series, greatly exceeding the 99% confidence limit for nonrandomness (F=6.93 for 2 and 12 degrees of freedom [see *Abramowitz and Stegun*, 1964]). Near 100-kyr period, the variance ratio peaks at $f \approx 7.9$ and 10.4 cycles/m.y. with values $F \gtrsim 4$. If there were a substantial stochastic "background" process in the $\delta^{18}O$ spectrum, values of F in this range could be interpreted as a modest phase coherent signal immersed in a "noise" process. However, the prominence of the 10 cycles/m.y. peak argues that the background spec-

TABLE 1. Data Series Used in This Study

Data Source	Data Type	Duration, m.y.	Δt, kyr	N
DSDP 607	benthic $\delta^{18}O$	2.75	3.5	787
ODP 677	benthic $\delta^{18}O$	2.6	3.0	865
ODP 677	planktonic $\delta^{18}O$	2.6	3.0	865
Berger [1978]	65°N insolation	3.0	2.0	1500
Berger and Loutre [1991]	65°N insolation	3.0	2.0	1500

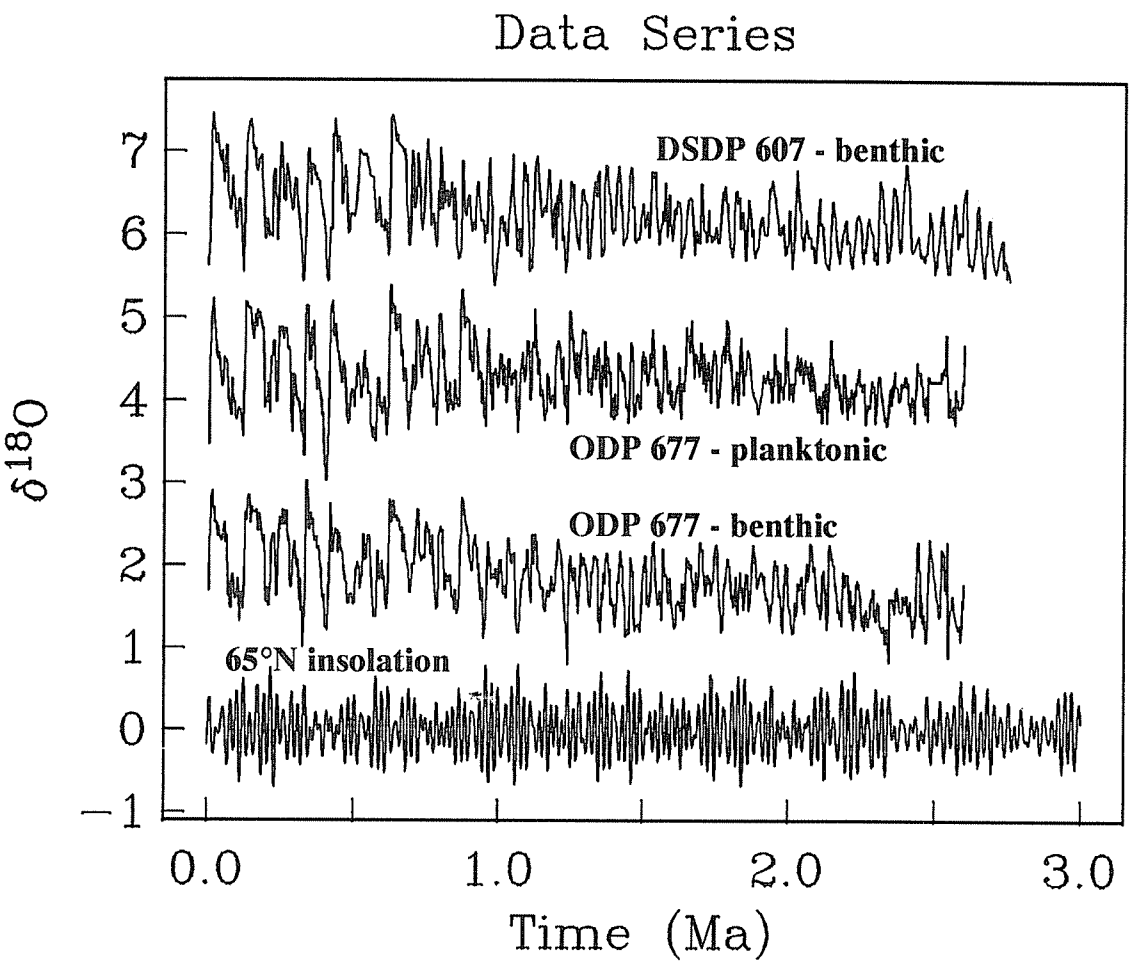

Fig. 5. The three $\delta^{18}O$ series used in this study, plotted with respect to their published time scales. The y ordinate is parts per thousand $\delta^{18}O$, and the series are shifted for clearer display. The time series of insolation at 65°N from *Berger and Loutre* [1991] is plotted for reference.

trum is fairly modest, and that the "signal" is not phase coherent throughout the duration of the series.

Figure 8 graphs the smooth envelope models for the obliquity band around $f_o = 24.4$ cycles/m.y., using seven 4π-prolate Slepian tapers and the penalty function (10). The series durations are in the range $2.5 < T \leq 3.0$ m.y., so that the Rayleigh frequencies are in the range $0.333 \leq f_R < 0.4$ cycles/m.y. The envelopes represent spectral information within a bandpass of width $2.6 < 8f_R < 3.2$ cycles/m.y., centered on carrier frequency f_o. This bandpass corresponds to the width of the boxy peak at the 41-kyr obliquity cycle in the spectra graphed in Figure 7. The tuned time scales for DSDP 607 and ODP 677 were developed using target curves derived from the "old" [*Berger*, 1978] and "new" [*Laskar*, 1988; *Berger and Loutre*, 1991] astronomical solutions, respectively. Data from DSDP 607, on the time scale proposed by *Ruddiman et al.* [1989], and *Raymo et al.* [1989], follow the phase variation of the *Berger* [1978] astronomical obliquity signal quite well, with a phase lag that corresponds to 13–14 kyr. The phase of the envelopes from ODP 677, using the time scale published by *Shackleton et al.* [1990], drifts relative to the 1978 astronomical series but follows the new astronomical obliquity solution quite well. (Benthic $\delta^{18}O$ is graphed, but planktonic $\delta^{18}O$ is similar.) It is readily apparent from these envelope phase estimates which time scale

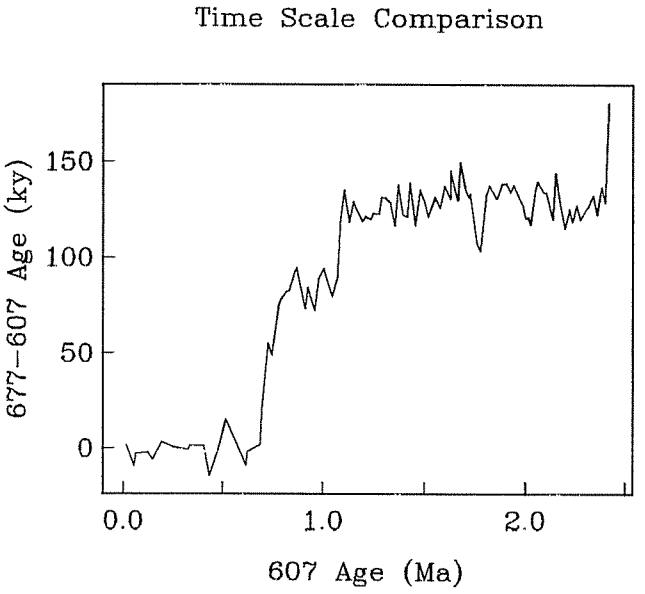

Fig. 6. The time shift between the time scales for ODP site 677, proposed by *Shackleton et al.* [1990], and DSDP site 607, as proposed by *Ruddiman et al.* [1989] and *Raymo et al.* [1989]. The correlations are obtained by visual identification of $\delta^{18}O$ isotope "stages" 1–100.

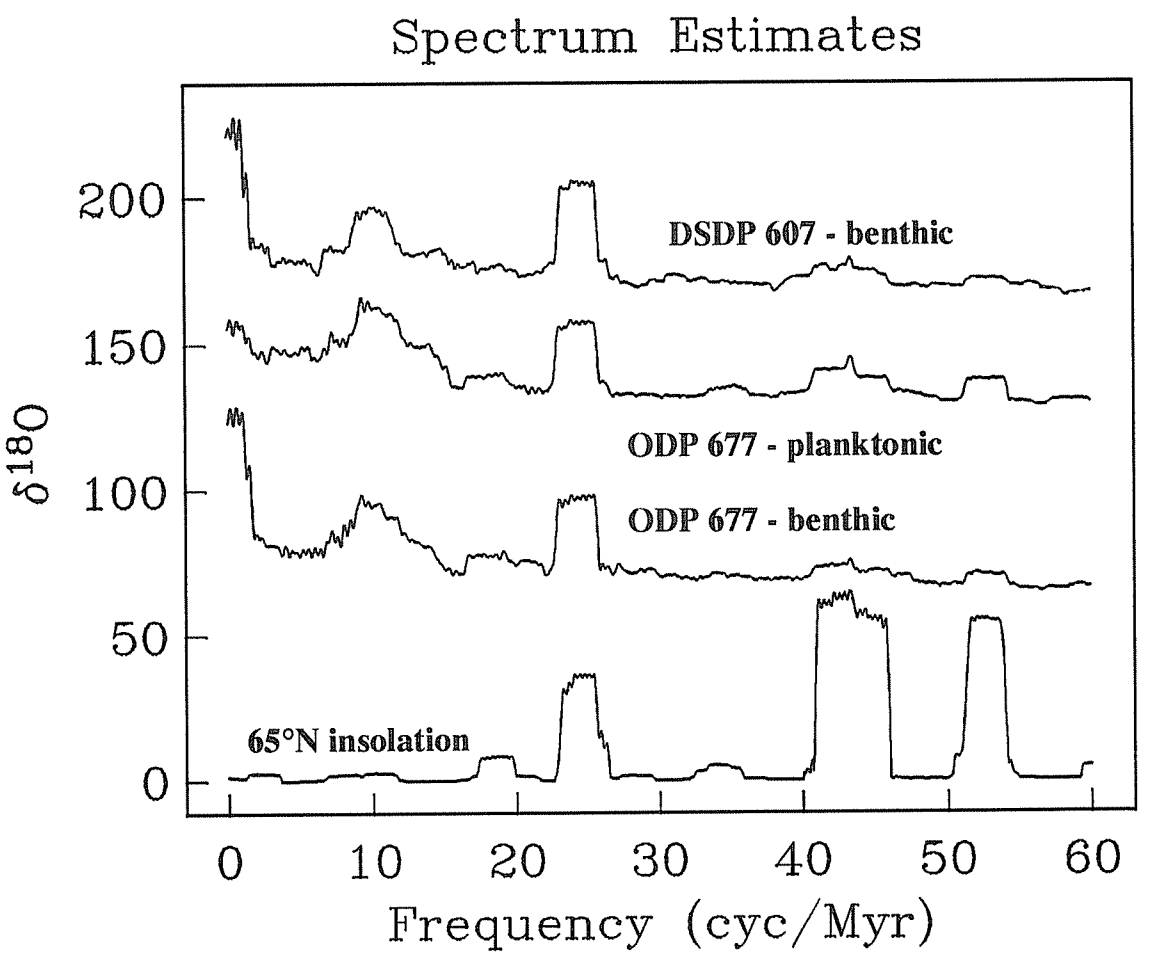

Fig. 7. Spectrum estimates of the three $\delta^{18}O$ series used in this study, calculated with respect to their published time scales. We graph the adaptive multiple-taper spectrum estimate, obtained using seven 4π-prolate Slepian eigentapers. The spectrum of the 65°N insolation series is plotted for reference.

was used in each case. When the benthic $\delta^{18}O$ data from DSDP site 607 are mapped onto the ODP 677 time scale using the isotope stage match curve shown in Figure 5, the phases of the two core's obliquity cycles match well (Figure 9). The phase agreement is perhaps expected, but more notable is the agreement of the envelope amplitudes since 2.2 Ma. On the Ruddiman/Raymo time scale, the obliquity cycle in the DSDP 607 data exhibits a maximum at 1.2 Ma, which drops to a minimum at 0.4 Ma. On the *Shackleton et al.* [1990] time scale, the maximum amplitude decreases, shifting to 1.4 Ma, and the 0.4 Ma minimum disappears. Both changes bring the time variation of the putative obliquity cycle in closer agreement with both the ODP 677 data and the new astronomical series. The agreement degrades somewhat for the end of the series, where the constraints offered by the envelope inversion are least constrained. Using the newer astronomical series and the *Shackleton et al.* [1990] time scale, for times < 2.2 Ma the $\delta^{18}O$ "response" to obliquity, as observed at DSDP site 607 and ODP site 677, is dominantly linear. In contrast, if we use the Ruddiman/Raymo time scale, the envelope of the putative obliquity signal from the DSDP 607 benthic $\delta^{18}O$ data differs significantly from the astronomical obliquity envelopes, and would require a more complicated relation between $\delta^{18}O$ fluctuations and obliquity insolation variations.

It is important to note that in the obliquity band, the statistical correlations among the data and astronomical time series are quite large, even without adjusting the time scale. Using the multiple-taper correlation measure described by *Vernon et al.* [1991], we obtain correlation coefficients $r > 0.9$ for all pairs of time series at $f_o = 24.35$ cycles/m.y., which validates the unspectacular assertion that the series are, to high confidence ($> 99\%$), statistically correlated at this frequency. Comparing the envelope inversions from different series, however, offers the analyst the opportunity to examine the correlation of two series as a function of time, so that departures from perfect correlation can be illuminated and (cautiously) interpreted.

The astronomical eccentricity series is dominated by quasi-periodic oscillations at (roughly) 95, 125, and 413 kyr (10.5, 8.0 and 2.42 cycles/m.y., respectively). The direct contribution of these cycles to the insolation received by Earth is weak, but eccentricity modulates the larger insolation signal associated with precession. The envelopes of the 94.8- and 124.2-kyr cycles (Figure 10) vary in tandem, when estimated simultaneously with seven 4π-prolate Slepian tapers, a constant-amplitude fixed element and roughness penalty (10). When this bandpass in the benthic $\delta^{18}O$ data from DSDP 607 is modelled in terms of envelopes of carrier frequencies 8.05 and 10.55 cycles/m.y. (Figure 11), poor correlation with the astronomical signal is found at ages greater than 1 Ma. For ages less than 1 Ma, the phases of both envelopes are stable and approximately 180° out of phase with the astronomical series. This phase relationship

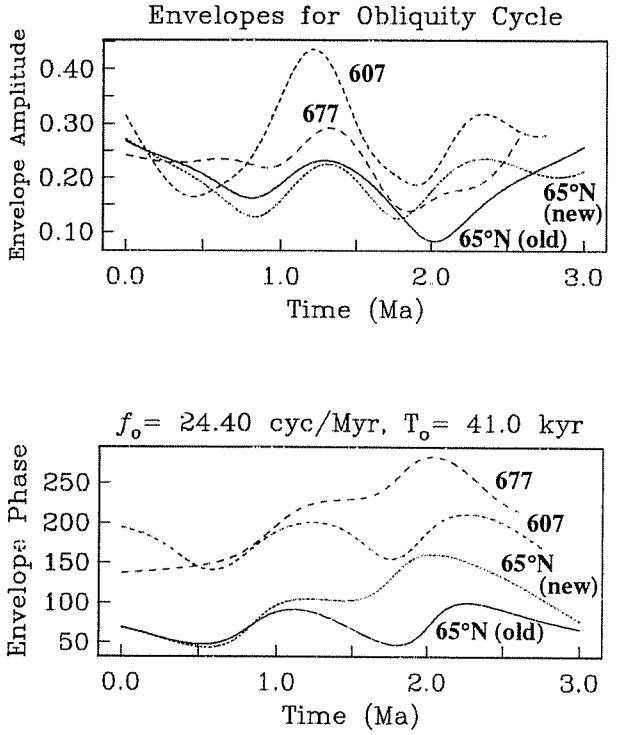

Fig. 8. Smooth envelope inversions for the time evolution of the 41-kyr signal in the benthic δ^{18}O series graphed in Figure 5, plotted against similar analyses for the astronomical insolation series derived from *Berger* [1978] ("65° old") and *Berger and Loutre* [1991] ("65°N new"). In this and succeeding plots, except where noted, seven 4π-prolate Slepian eigentapers are used to constrain the estimates, using smoothness penalty function (10). The amplitude units in this and succeeding plots are parts per thousand δ^{18}O . Note the phase correlation (due to orbital tuning) between the older astronomical series and data from DSDP site 607 and the correlation between the newer astronomical series and data from ODP site 677. Orbital tuning does not enforce correlations between envelope amplitudes, as is evident from the upper panel.

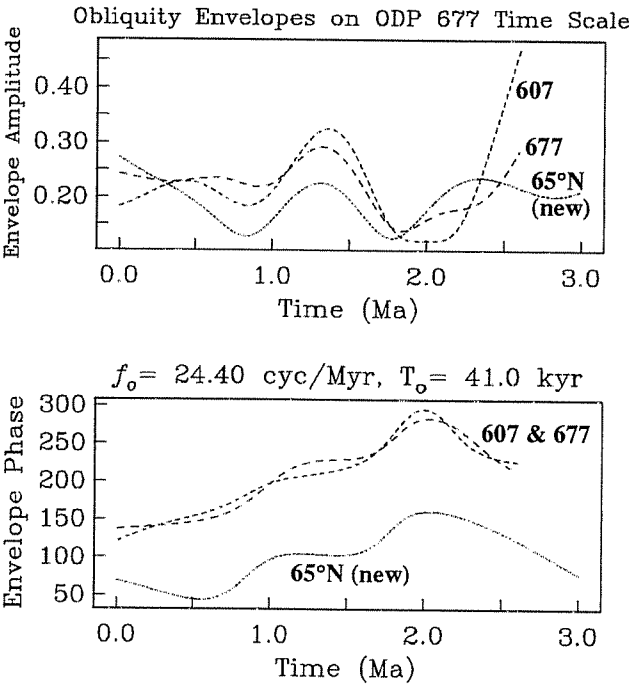

Fig. 9. Similar to Figure 8, but with the envelope of the *Berger* [1978] series omitted and benthic δ^{18}O data from DSDP site 607 expressed in terms of the *Shackleton et al.* [1990] time scale. Note the improved correlations between envelope amplitudes and phases.

correlates lighter isotopic values (i.e., decreased ice volume) with maxima in orbital eccentricity, that is, correlates large ice sheets with time intervals where precession insolation cycles are minimal. The growth of envelope amplitude for the 124-kyr quasi-period appears to start at 1.25 Ma. This growth is dwarfed by the growth of the 95-kyr envelope amplitude, which rises from zero at 1.0 Ma to a maximum at 0.45 Ma, then declines. The behavior of the 95-kyr envelope is broadly consistent with that reported by *Ruddiman et al.* [1989] for the 100-kyr bandpass. Multitaper envelope estimation allows us to model simultaneously the envelope of signal at the nearby 124-kyr eccentricity period.

Envelope inversions at precession frequencies f_o = 44.6 and 42.15 cycles/m.y. (periods of 23.7 and 22.4 kyr, respectively) support a link between the 100-kyr δ^{18}O cycle and other orbital cycles. Both these frequencies are characterized by F variance ratio peaks that suggest significant phase coherence. The envelopes, for ages less than 1.3 Ma, resemble the envelopes at the eccentricity frequencies (Figure 12). The insolation variation associated with precession is a summer/winter effect that is modulated by the eccentricity of Earth's orbit. In the frequency domain, this splits the insolation peak associated with Earth's (relatively) steady precession of figure into a collection of spectral lines whose frequencies differ by the eccentricity frequencies. For instance, the frequency differences between the precession peak at f = 52.7 cycles/m.y. (19.0-kyr period) and the peaks associated with the 23.7- and 22.4-kyr cycles correspond to the 95- and 124-kyr eccentricity peaks, respectively. In the benthic δ^{18}O data from DSDP 607 (on its published time scale), the envelope with carrier frequency f_o = 52.7

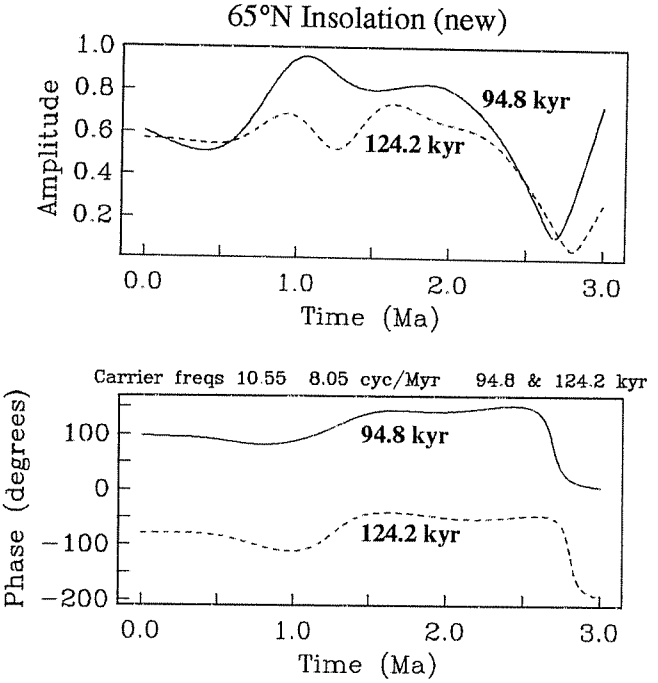

Fig. 10. Double-line smooth envelope inversion for the astronomical insolation series derived from *Berger and Loutre* [1991], at the two major eccentricity quasi-periods of 95 and 124 kyr. (The precise values were chosen to plot the envelope phases without a 360° "wraparound".)

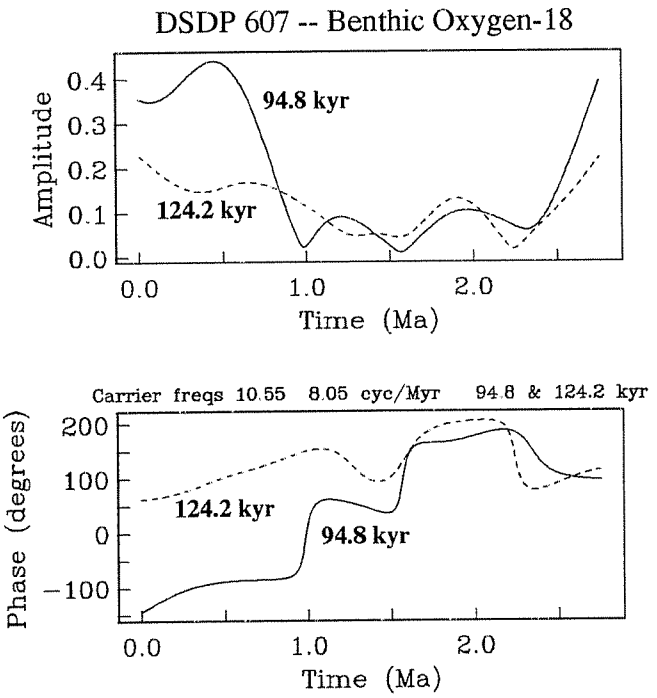

Fig. 11. Double-line smooth envelope inversion for the benthic δ^{18}O series from DSDP site 607 on its published time scale, at the two major eccentricity quasi-periods of 95 and 124 kyr.

cycles/m.y. varies only modestly for times $t \lesssim 1.5$ Ma. Therefore the one expects the interference of the three precession cycles in the DSDP 607 δ^{18}O data to resemble the envelopes at the eccentricity frequencies. The amplitudes at the precession frequencies are dwarfed by those of the eccentricity cycles at times $t < 1$ Ma, however.

The behavior of envelopes at eccentricity periods near 100 kyr, derived from δ^{18}O data from ODP site 677, is broadly similar (Figures 13 and 14). Envelope phases are fairly stable for $t < 1.2$ Ma. The growth of amplitude in the 100-kyr bandpass begins with the 124-kyr envelope, followed by rapid growth in the 95-kyr amplitude. Unlike the site 607 series, however, the 124-kyr envelope has a minimum at 0.4 Ma and appears to dominate the 95-kyr cycle in the last 200 kyr. Another distinction is the poor correlation of this behavior with the envelopes of the precession cycles at 44.6- and 42.15-kyr period. Both frequencies exhibit $F > 30$ in the spectral phase coherence test, and the envelope inversions corroborate that these precession cycles have fairly stable amplitudes and phases over the last 2.5 m.y. The precession cycles in the benthic δ^{18}O series from site 677 are less phase-coherent ($F \sim 6 - 10$), but neither do they correlate well with the envelopes of the 100-kyr eccentricity cycles graphed in Figures 13 and 14.

The correlation of envelopes among different δ^{18}O records should be substantial if, as is often hypothesized, the oxygen-isotope record indicates global ice volume directly. Differences among time series that cannot be explained by "background noise" or time scale discrepancies would force a search for other causative factors. When the DSDP 607 δ^{18}O data are mapped onto the ODP 677 time scale, the smooth envelope inversion for the 95- and 124-kyr eccentricity cycles correlates well with the envelopes derived from ODP 677 data, even for variations prior to 1 Ma (Figure 15). A phase match in the 100-kyr passband is not surprising in the late Pleistocene, since isotope stage matching aligns prominent events in the data. However, the timing of isotope stages prior to 0.8 Ma is governed primarily by the obliquity cycle, so that the match of the 95- and 124-kyr

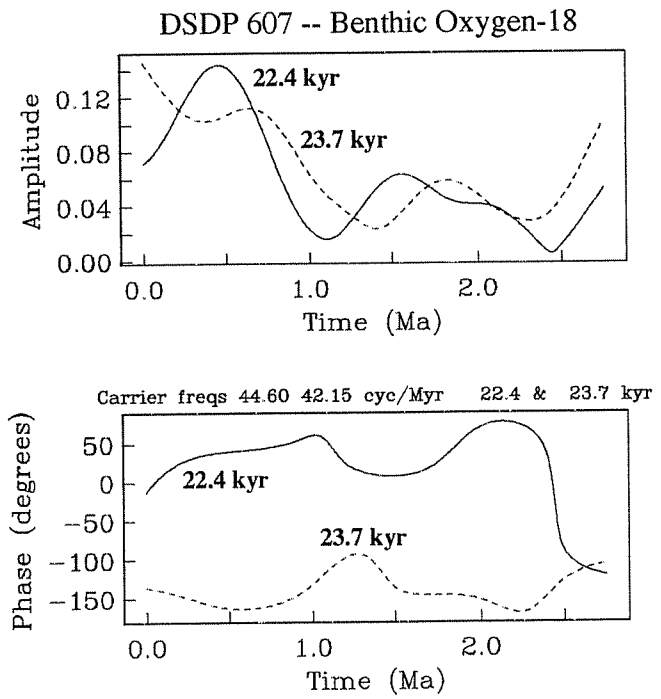

Fig. 12. Double-line smooth envelope inversion for the benthic δ^{18}O series from DSDP site 607 on its published time scale, at the two major precession quasi-periods of 22.4 and 23.7 kyr.

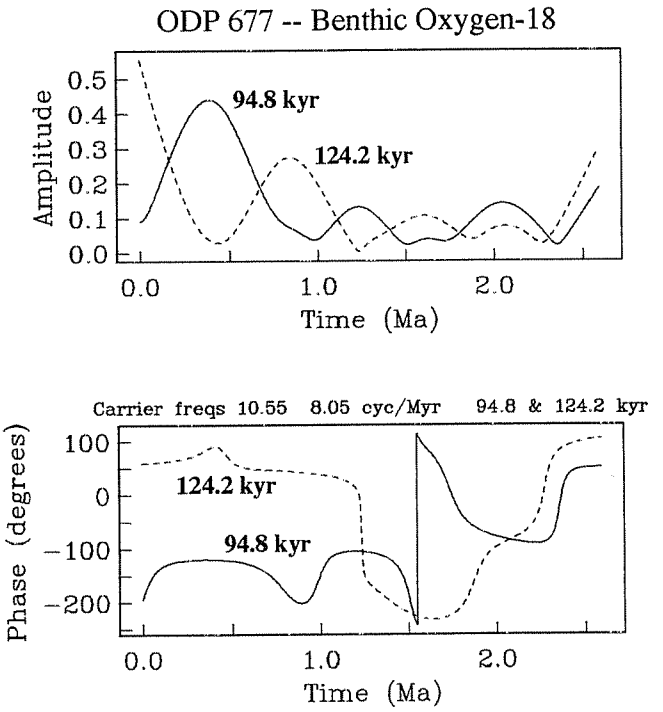

Fig. 13. Double-line smooth envelope inversion for the benthic δ^{18}O series from ODP site 677 on the *Shackleton et al.* [1990] time scale, at the two major eccentricity quasi-periods of 95 and 124 kyr.

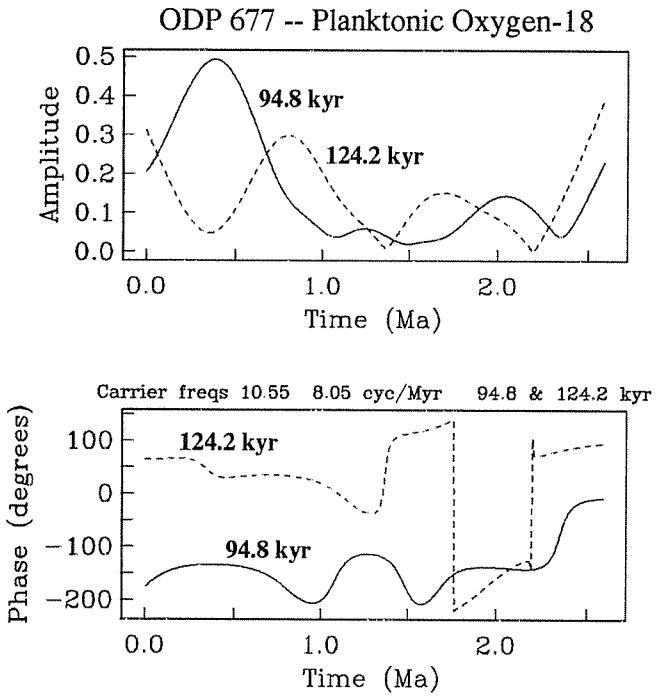

Fig. 14. Double-line smooth envelope inversion for the planktonic δ^{18}O series from ODP site 677 on the *Shackleton et al.* [1990] time scale, at the two major eccentricity quasi-periods of 95 and 124 kyr.

envelopes in this time interval is less likely to be an artifact of the rescaling technique. Moreover, the correlation of the rescaled 607 envelopes is stronger with envelopes from the benthic δ^{18}O series from site 677, suggesting a deep-ocean signal. This correlation, coupled with the correlation of the obliquity envelopes evident in Figure 9, suggests that a single causative factor is consistent with δ^{18}O fluctuations in these two deep-sea cores in the 100- and 41-kyr bandpasses.

The interpretation for the precession cycles is less straightforward. For DSDP 607 data on the ODP 677 time scale, the smoothest envelopes at carrier frequencies 44.6 and 42.15 cycles/m.y. do not correlate well with precession envelopes derived from ODP 677 data. Unresolved short-duration time scale inaccuracies could influence this comparison, as precession is the shortest of the orbital cycles. The adaptive multitaper spectrum estimate of the rescaled DSDP 607 data in the precession bandwidth shows considerable energy between the precession frequencies of 44.6 and 52.6 cycles/m.y. (22.4- and 19.0-kyr period). Additional tuning, beyond the isotope stage matching graphed in Figure 6, may increase the correlation of the site 607 δ^{18}O data with precession cycles in the astronomical series and with site 677 data. We experimented with different time scale mappings that fit the isotope stage correlations (Figure 6) with varying accuracy, but the effect on the precession envelopes was not great. Although these tests were not exhaustive, it appears probable that modest retuning will not improve the correlation significantly and that more than one factor influences the precession band in the DSDP 607 and ODP 677 δ^{18}O records.

Climate simulations with atmospheric general circulation models [*Prell and Kutzbach*, 1987; *Oglesby and Park*, 1989; *Park and Oglesby*, 1991] suggest that the precession cycle influences the precipitation-evaporation balance over low-latitude oceans. The associated changes in photic zone salinity would influence planktonic δ^{18}O values. Model simulations suggest that this low-latitude response to precession is predominantly linear [*Park and Oglesby*, 1991], which is consistent with the enhanced phase coherence of the precession cycles in the planktonic, compared to the benthic, δ^{18}O values from ODP 677. Therefore it is reasonable to hypothesize that δ^{18}O data from low-latitude site 677 should correlate less well with precessional ice volume cycles than would δ^{18}O data from the higher-latitude site 607.

The roughness penalty in the envelope inversion restricts our ability to model rapid changes in the envelope of the 100-kyr δ^{18}O cycles. Nonlinear climate models have been developed using the hypothesis that the 100-kyr ice age cycle arises from an instability in the Earth climate system. An abrupt onset of the 100-kyr ice age cycle characterizes these nonlinear climate models, arising from a bifurcation of the system from a stable to an unstable regime possessing a near 100-kyr free oscillation. This free oscillation is sensitive to, but not driven by, the external orbital insolation cycles. Such a bifurcation could explain the appearance of the 100-kyr cycle in the mid-Pleistocene in the absence of pronounced external forcing in the eccentricity passband [*Maasch and Saltzman*, 1990; *Saltzman and Maasch*, 1988, 1990, 1991].

An abrupt onset in the 95-kyr δ^{18}O envelope is consistent with the DSDP 607 δ^{18}O data series under certain conditions. Figure 16 shows results of smooth envelope inversions of the benthic δ^{18}O series from DSDP site 607 (on the Ruddiman/Raymo time scale) at f_o = 10.55 cycles/m.y., with discontinuities allowed at 0.7, 0.85, and 1.0 Ma. A discontinuity allowed at 1.0 Ma leads to an envelope similar to that

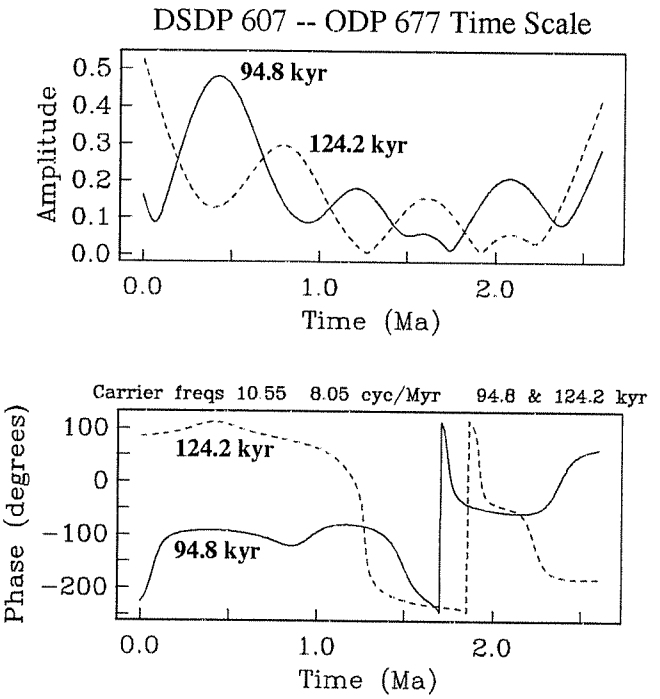

Fig. 15. Double-line smooth envelope inversion for the benthic δ^{18}O series from DSDP site 607 mapped onto the *Shackleton et al.* [1990] time scale, at the two major eccentricity quasi-periods of 95 and 124 kyr.

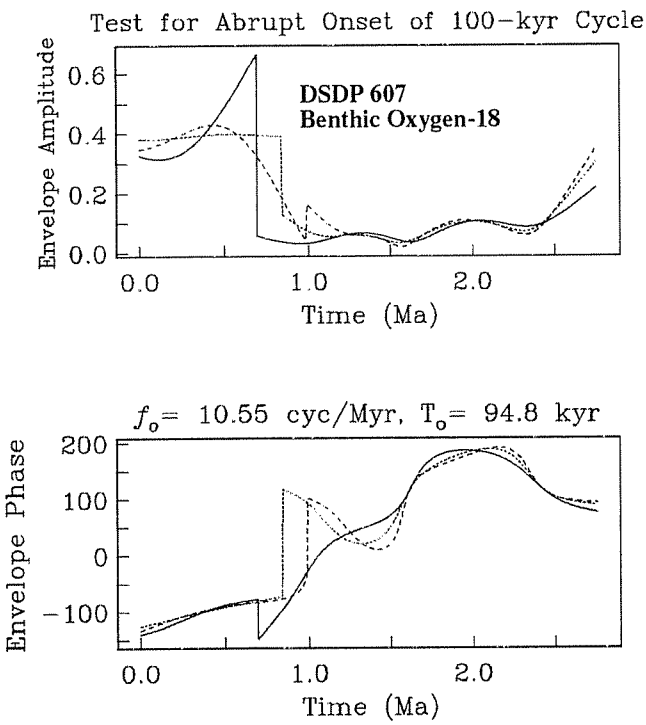

Fig. 16. Test for the abrupt onset of the 100-kyr signal. Envelope inversions for the benthic δ^{18}O series from DSDP site 607 on its published time scale, at the major eccentricity quasi-period 95 kyr. Seven 4π-prolate Slepian eigentapers are used to constrain the estimates, which are constrained to be smooth everywhere except at time points t_o =0.70, 0.85, and 1.00 Ma, respectively.

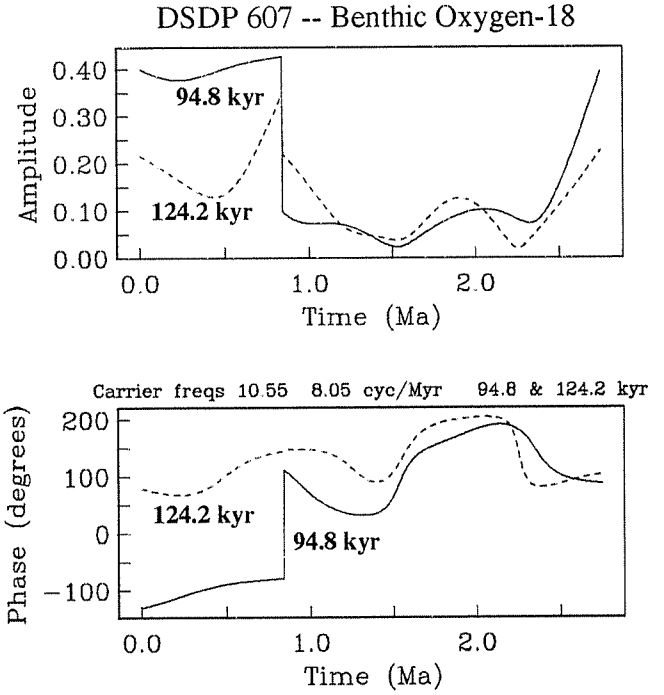

Fig. 17. Test for the abrupt onset of the 100-kyr signal. Double-line envelope inversion for the benthic δ^{18}O series from DSDP site 607 on its published time scale, at the two major eccentricity quasi-periods of 95 and 124 kyr. The envelopes are constrained to be smooth everywhere except at t_o =0.85 Ma.

shown in Figure 11. A discontinuity allowed at 0.7 Ma leads to an envelope with a sharp amplitude maximum at the discontinuity. Note that the phase of this envelope (long-dashed line in Figure 16) attempts to match phase across the discontinuity, suggesting that some 100-kyr signal with phase close to that of the astronomical cycle exists at ages greater than 0.7 Ma. By contrast, a discontinuity allowed at 0.85 Ma leads to an envelope with roughly constant amplitude at ages younger than 0.85 Ma and no anomalous deviation in phase at times older than the discontinuity. Based on this comparison, a sudden onset of the ice age cycle at 0.85 Ma, but not significantly earlier or later, appears to be a reasonable model for the narrow-band 100-kyr signal at site 607.

Figure 17 graphs a double-envelope inversion on the DSDP 607 δ^{18}O series with a discontinuity allowed at 0.85 Ma. A large jump in 95-kyr amplitude across the assumed discontinuity is evident. The envelope at carrier frequency f_o = 8.05 cycles/m.y. suffers a modest amplitude jump at the discontinuity, but its phase remains roughly 180° out of phase with the 124-kyr astronomical eccentricity cycle across the discontinuity. The amplitude of the 124-kyr envelope is smaller than that of the 95-kyr envelope at its peak, but it is significant. Unless this phase agreement is fortuitous, Figure 17 describes a climate system which shifts abruptly to lock phase and amplitude with one eccentricity cycle while its behavior at an adjacent eccentricity cycle is largely unchanged.

A further caveat in the abrupt onset hypothesis is motivated by Figure 6. The greatest relative shifts in the published time scales of sites 607 and 677, as determined by isotope stage matching, occur between 0.7 Ma and 1.2 Ma.

It is not difficult to argue that distortions of this magnitude could introduce spurious features into the envelope inversion. This argument is strengthened by Figure 18, which graphs a double-envelope inversion on the ODP 677 ben-

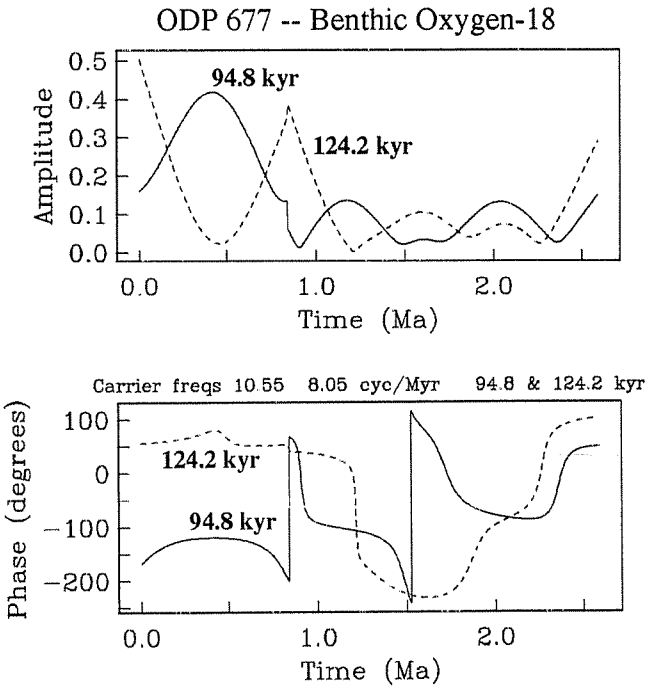

Fig. 18. Double-line envelope inversion for the benthic δ^{18}O series from ODP site 677 on the *Shackleton et al.* [1990] time scale, at the two major eccentricity quasi-periods of 95 and 124 kyr. The envelopes are constrained to be smooth everywhere except at t_o =0.85 Ma.

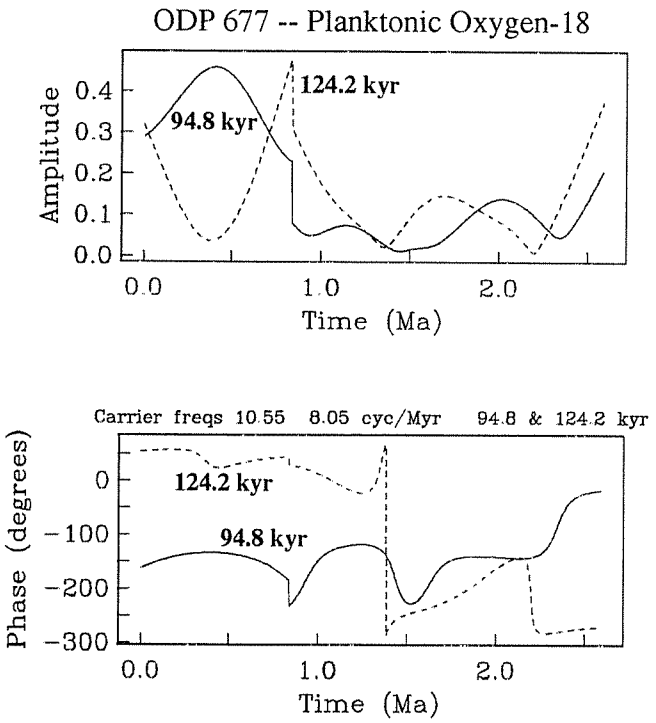

Fig. 19. Double-line envelope inversion for the planktonic $\delta^{18}O$ series from ODP site 677 on the *Shackleton et al.* [1990] time scale, at the two major eccentricity quasi-periods of 95 and 124 kyr. The envelopes are constrained to be smooth everywhere except at t_o =0.85 Ma.

thic $\delta^{18}O$ series with a discontinuity allowed at 0.85 Ma. A discontinuity in either the 95- or 124-kyr envelopes is not preferred by the analysis. Similar results are obtained if, consistent with the shift in time scale between sites 677 and 607, the discontinuity is shifted to 0.9 or 0.95 Ma. Double-envelope inversions using the ODP 677 planktonic $\delta^{18}O$ series (Figure 19) and the DSDP 607 $\delta^{18}O$ series on the ODP 677 time scale (not shown) interpolate the behaviors seen in Figures 17 and 18: an abrupt jump in the 95-kyr envelope appears consistent with the data (but less persuasive than in Figure 17), but appears unnecessary to describe the 124-kyr envelope. We also examined the composite envelope formed by the beating interference of the two cycles. In both continuous and discontinuous envelope inversions at the eccentricity frequencies using the *Shackleton et al.* [1990] time scale, the cycles interfere so as to produce a minimum signal near 0.75 Ma, after the "sudden onset" of 95-kyr signal modelled in Figure 17.

The site 677 time scale leads to a simpler relationship between orbital cycles and the $\delta^{18}O$ record than does the site 607 time scale and does not favor an abrupt onset of the 100-kyr $\delta^{18}O$ cycle in the mid-Pleistocene. Although Occam's Razor would argue for the simpler behavior, the internal evidence in the $\delta^{18}O$ time series does not discriminate conclusively between the time scales. Other constraints are necessary. The *Shackleton et al.* [1990] time scale pushes the Brunhes-Matayama magnetic reversal to 0.78 Ma, some 40-50 kyr older than previously published radiometric dates. No such adjustment is necessary if the published time scale for site 607 data is accepted. Milankovitch tuning of some other sedimentary records, however, has suggested age shifts similar to those suggested by *Shackelton et al.* [1990]. *Johnson* [1982] proposed an age of 0.79 Ma for the Brunhes-Matayama reversal based on older, shorter $\delta^{18}O$ series. *Hilgen and Langereis* [1989] proposed age shifts for several magnetic reversals on the basis of Milankovitch tuning of Pliocene sedimentary sequences in Sicily. Using an improved laser fusion ^{40}Ar–^{39}Ar dating method on sanidine samples from the Bishop Tuff, California, *Izett and Obradovich* [1991] revised their radiometric age estimate for the Brunhes-Matayama reversal to 0.79 Ma. *Spell and McDougall* [1992] infer a date for the reversal of 0.78±0.01 Ma by dating sanidine samples from the Valles Caldera, New Mexico. If the *Shackleton et al.* [1990] time scale is further confirmed, the existence of a globally coherent low-amplitude 100-kyr $\delta^{18}O$ cycle prior to its dominance in the late Pleistocene is strongly supported by our analysis.

SUMMARY

The variation of climate proxy variables at a given frequency f_o (with associated period $T_o = 1/f_o$) can be parameterized by $\Re\{A(t)e^{-2\pi i f_o t}\}$, a sinusoid with a slowly varying amplitude $A(t)$. The function $A(t)$ is complex-valued, allowing slow variations in phase as well as magnitude. We define $A(t)$ as the envelope of the signal at "carrier frequency" f_o. If $A(t) = A_o$ is a constant, the signal is termed "periodic" or "a phase coherent sinusoid." If $A(t)$ varies, the signal is termed "quasi-periodic." All methods for estimating the envelope of a quasi-periodic signal have shortcomings. Bandpass filters, such as those used by *Ruddiman et al.* [1989], cannot model discontinuities in the envelope of a quasi-periodic signal and thus, are of little help in discriminating between a sudden and a gradual onset for the 100-kyr ice age cycle. Moreover, a narrow bandpass in the frequency domain requires a long time domain filter, so that a significant number of data points at the ends of the series must be discarded. Similarly, the choice of length for the overlapping data segments in the *Ruddiman et al.* [1986b] analysis involves a trade-off between frequency and time resolution.

We apply instead a more flexible approach based on multiple-taper spectral analysis [*Thomson*, 1982, 1990; *Park et al.*, 1987; *Berger et al.*, 1991; *Vernon et al.*, 1991]. The multitaper approach allows the analyst to model the envelope function $A(t)$ using the tools of linear inverse theory, solving for the envelope function that fits the time series data while optimizing a chosen property of the envelope. Inversion algorithms can be derived that find the smallest and smoothest envelopes that fit spectral data from a given time series. Special cases of these algorithms can be derived to model sudden changes in the envelope. This allows us to hypothesize an abrupt onset of the 100-kyr periodicity, as well as to examine the evolution of the obliquity and precession signals. The estimation procedure relates spectrum estimates at f_o, using a set of orthogonal Slepian tapers, as linear functionals of an unknown envelope $A(t)$, so that the envelope is constructed from a linear combination of the Slepian tapers. Since the Slepian tapers are optimally bandlimited, multitaper envelope estimation can be thought of as an extremely sharp narrow-band filter valid for the entire duration of the series.

The shortcomings of the algorithm we use are similar to those of other linear inverse problems. For instance, the multitaper envelope estimation procedure can model envelope discontinuities, but the technique cannot by itself discriminate between continuous and discontinuous models for the 100-kyr cycle, since envelopes of both types can be con-

structed that fit the spectral data exactly. The analyst must use other, perhaps subjective, criteria for choosing among models that fit the data. This nonuniqueness is a common problem in linear inverse theory; in principle, an infinite number of envelopes can fit a finite number of spectral data exactly. In most cases, the a priori constraint that the signal at a carrier frequency f_o have a "slowly varying" envelope, except at one or more specified time points, reduces greatly the range of acceptable models for the envelope, and motivates solving for the smoothest envelope that fits the spectral data.

We investigated the time evolution of the 100-kyr cycle in δ^{18}O data, thought to reflect global ice volume variations. We analyzed δ^{18}O data from DSDP site 607 and ODP site 677, from which three long (> 2.6 m.y.) time series have been published. We find evidence for a coherent δ^{18}O signal for both cores in the eccentricity and obliquity frequency bands, consistent with variations in global ice volume as the causative factor. However, the nature of the Earth system response to orbital insolation cycles depends on the time scale adopted in the spectral analysis. If the *Shackleton et al.* [1990] time scale for ODP site 677 is accepted, a linear Earth system response to orbital obliquity is suggested by our analysis, because the amplitude of the δ^{18}O obliquity cycle matches well the 65°N obliquity insolation derived by *Berger and Loutre* [1991] for times $t \lesssim 2.3$ Ma. (The phase match for obliquity is enhanced by the fact that the data series were tuned to the astronomical time series, so that the observed phase agreement is not surprising.) If the Ruddiman/Raymo time scale for DSDP site 607 is accepted, the δ^{18}O obliquity cycle has enhanced amplitude between 1.0 and 1.5 Ma, relative to the late Pleistocene ($t < 1.0$ Ma), and a nonlinear response of the Earth system to orbital obliquity is suggested.

After analyzing of data from these two deep-sea cores, we do not find compelling evidence for an abrupt change in the 100-kyr δ^{18}O signal. Rather, envelope inversions in the eccentricity band suggest that the 100-kyr δ^{18}O cycle is phase locked with the 124-kyr eccentricity cycle some 300-400 kyr prior to its late Pleistocene growth in amplitude and phase lock with the 95-kyr eccentricity cycle. An abrupt change in the 95-kyr envelope near 0.85 Ma is consistent with DSDP 607 data on the Ruddiman/Raymo time scale, but such a transition would occur while leaving the 124-kyr envelope largely unchanged. If the *Shackleton et al.* [1990] time scale for ODP 677 is accepted, our three δ^{18}O records are consistent with a low-amplitude 100-kyr cycle between 1.2 and 2.6 Ma, whose local period of oscillation alternates between the two major eccentricity periods at 95 and 124 kyr. The phase of these 100-kyr oscillations prior to 1.2 Ma is related to the phase of the astronomical eccentricity cycles where the cycles have significant amplitude (e.g., Figure 20). The match between the precessional envelopes of sites 607 and 677 is poor, when both are expressed in terms of the *Shackleton et al.* [1990] time scale. Climate simulation studies suggest that cyclic salinity changes in equatorial surface waters are a plausible contributor to the ODP 677 δ^{18}O data in the precessional band, and could explain this discrepancy.

Further study of more paleoclimate records will be necessary to address more fully the time evolution of the 100 kyr cycle. For instance, the correlation of δ^{18}O signals from sites 677 and 607 is intriguing, but comprehensive tests for the global coherence of δ^{18}O signals should use data from more than two sites. The phase information contained in the

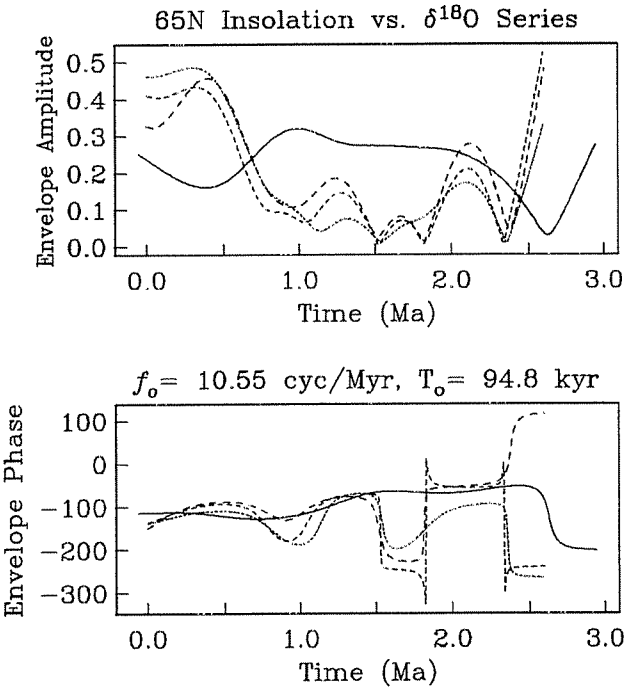

Fig. 20. Solid curve: smooth envelope inversion for the astronomical insolation series derived from *Berger and Loutre* [1991], at the major eccentricity quasi-period 95 kyr. Dashed curves: smooth envelope inversions, at the same carrier frequency, for the three δ^{18}O series used in this study. Fine-, medium-, and long-dashed curves correspond to ODP 677 planktonic δ^{18}O, ODP 677 benthic δ^{18}O, and DSDP 607 benthic δ^{18}O, respectively. Seven 4π-prolate Slepian eigentapers are used to constrain the envelopes. The envelope corresponding to the 65°N curve is time shifted by 55 kyr (phase-shifted by 150°) to facilitate comparison. Note that phase agreement between the astronomical series and the δ^{18}O data is good in the time intervals 0.0–0.8 Ma, 1.1–1.5 Ma, and 1.8–2.3 Ma, where the amplitude of the δ^{18}O envelopes is maximal.

paleoclimate records may reaffirm the notion that external Earth-orbital forcing is the pacemaker of the ice age cycles and validate the suggestion that the influence of eccentricity cycles was significant prior to the late Pleistocene. However, the mid-Pleistocene amplitude increase of the quasi-periodic 100-kyr δ^{18}O signal awaits a complete explanation, which appears to depend on factors other than orbital insolation cycles.

Acknowledgments. We thank Maureen Raymo and Nicholas Shackleton for help in obtaining copies of their data series, and J. Laskar for floppies of his most recent astronomical series. We thank Barry Saltzman and Robert J. Oglesby for helpful comments and Philip Stark and Robert L. Parker for constructive reviews. This work has received support from NSF grants EAR-8657206 and ATM-8802630, as well as NASA grant NAG8-785.

REFERENCES

Abramowitz, M., and I. A. Stegun (Eds.), *Handbook of Mathematical Functions*, National Institute of Standards and Technology, Gaithersburg, Md., 1964.

Berger, A., A simple algorithm to compute long-term variations of daily or monthly insolation, *Contrib. 18, Universite Catholique de Louvain,* Inst. Astron. Geophys. G. Lemaitre, 17 pp, 1978.

Berger, A., and M. F. Loutre, Insolation values for the climate of the last 10 million years, *Quat. Sci. Rev., 10,* 297–317, 1991.

Berger, A., J. L. Melice, and L. Hinnov, A strategy for frequency

spectra of Quaternary climate records, *Clim. Dyn.*, *5*, 227–240, 1991.

Constable, C. G., and R. L. Parker, Smoothing, splines and smoothing splines, *J. Comput. Phys.*, *78*, 493–508, 1988.

Constable, S. C., R. L. Parker, and C. G. Constable, Occam's inversion: A practical algorithm for generating smooth models from electromagnetic sounding data, *Geophysics*, *52*, 289–300, 1987.

DeBlonde, G., and W. R. Peltier, A model of late Pleistocene ice sheet growth with realistic geography and simplified cryodynamics and geodynamics, *Clim. Dyn.*, *5*, 103–110, 1990.

DeBlonde, G., and W. R. Peltier, A one-dimensional model of continental ice volume fluctuations through the Pleistocene: Implications for the origin of the mid-Pleistocene climate transition, *J. Clim.*, *4*, 318–344, 1991.

Hilgen, F. J., and C. G. Langereis, Periodicities of $CaCO_3$ cycles in the Pliocene of Sicily: Discrepancies with the quasi-periods of the Earth's orbital cycles?, *Terra Nova*, *1*, 409–415, 1989.

Imbrie, J.I., and J.Z. Imbrie, Modelling climate response to orbital variations, *Science*, *207*, 943–953, 1980.

Imbrie, J., J. D. Hays, D. G. Martinson, A. McIntyre, A. C. Mix, J.J. Morley, N. G. Pisias, W. L. Prell, and N. J. Shackleton, The orbital theory of Pleistocene climate: support from a revised chronology of the marine $\delta(^{18}O)$ record, in *Milankovitch and Climate, Part 1*, edited by A. Berger, J. Imbrie, J. Hays, G. Kukla, and B. Saltzman, pp. 269–306, D. Riedel, Hingham, Mass., 1984.

Izett, G. A., and J. D. Obradovich, Dating of the Matayama-Brunhes boundary based on ^{36}Ar–^{40}Ar ages of the Bishop Tuff and Cerro San Luis Rhyolite (abstract), *Geol. Soc. Am. Abstr. Programs*, *23*, A106, 1991.

Johnson, R. G., Brunhes-Matayama magnetic reversal dated at 790,000 yr B. P. by marine-astronomical correlations, *Quat. Res.*, *17*, 135–147, 1982.

Laskar, J., Secular evolution of the solar system over 10 million years, *Astron. Astophys.*, *198*, 341–362, 1988.

Laskar, J., The chaotic motion of the solar system: A numerical estimate of the size of the chaotic zones, *Icarus*, *88*, 266–291, 1990.

Le Treut, H., and M. Ghil, Orbital forcing, climatic interactions, and glaciation cycles, *J. Geophys. Res.*, *88*, 5167–5190, 1983.

Maasch, K. A., Statistical detection of the mid-Pleistocene transition, *Clim. Dyn.*, *2*, 133–143, 1988.

Maasch, K. A., and B. Saltzman, A low-order dynamical model of global climate variability over the full Pleistocene, *J. Geophys. Res.*, *95*, 1955–1963, 1990.

Matteucci, G., A study of the climatic regimes of the Pleistocene using a stochastic resonance model, *Clim. Dyn.*, *6*, 67–81, 1991.

Menke, W., *Geophysical Data Analysis: Discrete Inverse Theory*, Academic, San Diego, Calif., 1984.

Oglesby, R. J., and J. Park, The effect of precessional insolation changes on Cretaceous climate and cyclic sedimentation, *J. Geophys. Res.*, *94*, 14,793–14,816, 1989.

Park, J., Observed envelopes of seismic free oscillations, *Geophys. Res. Lett.*, *17*, 1489–1492, 1990.

Park, J., Envelope estimation for quasi-periodic geophysical signals in noise: A multitaper approach, *Statistics in the Environmental & Earth Sciences*, edited by A. T. Walden and P. Guttorp, pp. 189–219, Edward Arnold, London, 1992.

Park, J., and T. D. Herbert, Hunting for paleoclimatic periodicities in a geologic time series with an uncertain time scale, *J. Geophys. Res.*, *92*, 14,027–14,040, 1987.

Park, J., and R. J. Oglesby, Milankovitch rhythms in the Cretaceous: A GCM modelling study, *Palaeogeogr. Palaeoclimatol. Palaeoecol.*, *90*, 329–355, 1991.

Park, J., C. R. Lindberg, and F. L. Vernon III, Multiple-taper spectral analysis of high frequency seismograms, *J. Geophys. Res.*, *92*, 12,675–12,684, 1987.

Parker, R. L., Understanding inverse theory, *Annu. Rev. Earth Planet. Sci.*, *5*, 35–64, 1977.

Pisias, N. G., and T. C. Moore, The evolution of Pleistocene climate: A time series approach, *Earth Planet. Sci. Lett.*, *52*, 450–458, 1981.

Prell, W. L., and J. E. Kutzbach, Variability of the monsoon over the past 150,000 years: Comparison of observed and simulated paleoclimatic time series, *J. Geophys. Res.*, *92*, 8411–8425, 1987.

Raymo, M. E., W. F. Ruddiman, J. Backman, B. M. Clement, and D. G. Martinson, Late Pliocene variation in northern hemisphere ice sheets and North Atlantic Deep Water circulation, *Paleoceanography*, *4*, 413–446, 1989.

Reinsch, C. H., Smoothing by spline functions, *Numerische Mathematik*, *10*, 177–183, 1967.

Ruddiman W. F., A. McIntyre, and M. Raymo, Paleoenvironmental results from North Atlantic sites 607 and 609, *Initial Rep. Deep Sea Drill. Proj.*, *94*, 855–878, 1986*a*.

Ruddiman W. F., M. Raymo, and A. McIntyre, Matuyama 41,000-year cycles: North Atlantic Ocean and northern hemisphere ice sheets, *Earth Planet. Sci. Lett.*, *80*, 117–129, 1986*b*.

Ruddiman, W. F., M. E. Raymo, D. G. Martinson, B. M. Clement, and J. Backman, Pleistocene evolution: Northern hemisphere ice sheets and the North Atlantic Ocean, *Paleoceanography*, *4*, 353–412, 1989.

Saltzman, B., and K. A. Maasch, Carbon cycle instability as a cause of the late Pleistocene ice age oscillations: Modeling the asymmetric response, *Global Biogeochem. Cycles*, *2*, 177–185, 1988.

Saltzman, B., and K. A. Maasch, A first-order global model of late Cenozoic climatic change. *Trans. R. Soc. Edinburgh*, *81*, 315–325, 1990.

Saltzman, B., and K. A. Maasch, A first–order global model of late Cenozoic climatic change II: A simplification of CO_2 dynamics, *Clim. Dyn.*, *5*, 201–210, 1991.

Saltzman, B., and A. Sutera, The mid-Quaternary climatic transition as the free response of a three-variable dynamical model, *J. Atmos. Sci.*, *44*, 236–241, 1987.

Shackleton, N. J., and M. A. Hall, Stable isotope history of the Pleistocene at ODP site 677, *Proc. Ocean Drill. Program Sci. Results*, *111*, 295–316, 1989.

Shackleton N. J., and N. D. Opdyke, Oxygen–isotope and paleomagnetic stratigraphy of Pacific core V28–239 late Pliocene to latest Pleistocene, in Investigations of Late Quaternary Paleoceanography and Paleoclimatology, edited by R. M. Cline and J. D. Hays, *Mem. Geol. Soc. Am.*, *145*, 449–464, 1976.

Shackleton, N. J., et al., Oxygen isotope calibration of the onset of ice–rafting and history of glaciation in the North Atlantic region, *Nature*, *307*, 620–623, 1984.

Shackleton, N. J., A. Berger, and W. R. Peltier, An alternative astronomical calibration of the lower Pleistocene timescale based on ODP site 677, *Trans. R. Soc. Edinburgh*, *81*, 251–261, 1990.

Shure, L., R. L. Parker, and G. E. Backus, Harmonic splines for geomagnetic modelling, *Phys. Earth Planet. Int.*, *28*, 215–229, 1982.

Slepian, D., Some comments on Fourier analysis, uncertainty, and modeling, *SIAM Rev.*, *25*, 379–393, 1983.

Spell, T. L., and I. McDougall, Revisions to the age of the Brunhes-Matayama boundary and the Pleistocene geomagnetic polarity time scale, *Geophys. Res. Lett.*, *19*, 1181–1184, 1992.

Start, G. G., and W. L. Prell, Evidence for two Pleistocene climatic modes: Data from DSDP site 502, in New Perspectives in Climate Modelling, edited by A. L. Berger and C. Nicolis, *Dev. Atmos. Sci.*, *16*, 3–22, 1984.

Thomson, D. J., Spectrum estimation and harmonic analysis, *IEEE Proc.*, *70*, 1055–1096, 1982.

Thomson, D. J., Quadratic-inverse spectrum estimates: Applications to paleoclimatology, *Philos. Trans. R. Soc. London*, *332*, 539–597, 1990.

Vernon, F. L., J. Fletcher, L. Carroll, A. Chave and E. Sembrera, Coherence of seismic body waves from local events as measured by a small-aperture array, *J. Geophys. Res.*, *96*, 11,981–11,996, 1991.

K. A. Maasch, Institute for Quaternary Studies, 320 Boardman Hall, University of Maine, Orono, ME 04468.

J. Park, Department of Geology and Geophysics, Box 6666, Yale University, New Haven, CT 06511.

(Received December 30, 1991;
revised July 15, 1992;
accepted July 20, 1992.)